Innovations in VLSI Architecture and Digital Signal Processing

Dr. M. KAMARAJAN
Mrs. DIMPLE JUNEJA
Dr. A. YOGESHWARAN
Dr. S. MUTHURAJAN

SRR
Publicizing Research

ISBN 978-816860178-9

Innovations in VLSI Architecture and Digital Signal Processing

April 2026

Dr. M. KAMARAJAN
Assistant Professor
Department of Electronics and Communication Engineering
Vels Institute of Science, Technology & Advanced Studies
Chennai, Tamil Nadu, India.

Mrs. DIMPLE JUNEJA
Research Scholar, Department of Education
Mohanlal Sukhadia University
Udaipur, Rajasthan, India.

Dr. A. YOGESHWARAN
Associate Professor
Department of Electronics and Communication Engineering,
Dhanalakshmi Srinivasan Engineering College
Perambalur, Tamil Nadu, India.

Dr. S. MUTHURAJAN
Assistant Professor, Department of Marine Engineering
Academy of Maritime Education and Training (AMET)
Deemed to be University
Chennai, Tamil Nadu, India.

April 2026

ISBN: 978-81-686017-8-9

© Copyrights reserved by Authors and Publishers

Despite our best efforts, there is still a risk that some errors and omissions might occur unintentionally.

Without the prior consent of the authors and publishers, no part of this publication may be duplicated in any form or by any means, whether electronically, by photocopying, or otherwise.

The opinions and findings expressed in the individual chapters are those of the authors and the book's editors, not the publishers.

Images attributed from www.freepik.com, www.quillbot.com

Published By

SRR
Publicizing Research

SCIENTIFIC RESEARCH REPORTS
(A Book Publisher, approved by Govt. of India)

I Floor, S S Nagar, Chennai - 600 087,
Tamil Nadu, India.

editors@srrbooks.in, contact@srrbooks.in
www.srrbooks.in

PREFACE

The rapid evolution of semiconductor technology and computational intelligence has significantly transformed the landscape of Very Large Scale Integration (VLSI) and Digital Signal Processing (DSP). The convergence of these domains has enabled the development of highly efficient, scalable, and intelligent systems that power modern applications ranging from communication and healthcare to artificial intelligence and embedded systems. This book, *Innovations in VLSI Architecture and Digital Signal Processing*, aims to present a comprehensive and structured exploration of contemporary advancements and emerging trends in these critical fields.

The first section, *Advanced VLSI Design Methodologies*, focuses on modern design paradigms that address increasing circuit complexity, reduced feature sizes, and stringent performance constraints. It highlights the role of design automation, verification strategies, and system-level integration in achieving reliable and optimized chip designs.

The second section, *Low-Power and High-Performance Architectures*, examines techniques to balance power efficiency with computational speed. As energy consumption becomes a critical concern in portable and large-scale systems alike, innovative architectural strategies and power-aware design techniques are essential for sustainable development.

In *Digital Signal Processing Algorithms and Hardware*, the book explores the interplay between algorithmic efficiency and

hardware realization. It emphasizes optimized implementations of DSP algorithms that are tailored for real-time processing and resource-constrained environments.

The section on *FPGA and ASIC Implementation Techniques* provides insights into practical design flows, prototyping strategies, and hardware realization approaches. It discusses how reconfigurable and application-specific platforms can be leveraged for rapid development and high-performance solutions.

With the increasing integration of artificial intelligence, *AI-Driven VLSI and DSP Optimization* introduces machine learning techniques applied to design automation, performance prediction, and adaptive system optimization. This interdisciplinary approach is shaping the future of intelligent electronic systems.

Finally, *Emerging Trends in Nanoelectronics and DSP Systems* highlights breakthroughs in nanoscale technologies, novel materials, and next-generation architectures. These advancements are expected to redefine the limits of performance, scalability, and functionality in electronic design.

This book is intended for researchers, academicians, and industry professionals seeking a deeper understanding of modern VLSI and DSP systems. It serves as both a reference and a guide to navigating the challenges and opportunities in this rapidly advancing domain.

We extend our sincere thanks to our publisher, Scientific Research Reports, Chennai, India, for their dedicated efforts in preparing this book and for ensuring the inclusion of enriched and high-quality technical content.

Wishes and Regards,

Dr. M. KAMARAJAN
Assistant Professor
Department of Electronics and Communication Engineering
Vels Institute of Science, Technology & Advanced Studies
Chennai, Tamil Nadu, India.

Mrs. DIMPLE JUNEJA
Research Scholar, Department of Education
Mohanlal Sukhadia University
Udaipur, Rajasthan, India.

Dr. A. YOGESHWARAN
Associate Professor
Department of Electronics and Communication Engineering,
Dhanalakshmi Srinivasan Engineering College
Perambalur, Tamil Nadu, India.

Dr. S. MUTHURAJAN
Assistant Professor, Department of Marine Engineering
Academy of Maritime Education and Training (AMET)
Deemed to be University
Chennai, Tamil Nadu, India.

SRR
Publicizing Research

CONTENTS

Section No	Section Titles	Page No
1	Advanced VLSI Design Methodologies	1-16
2	Low-Power and High-Performance Architectures	17-32
3	Digital Signal Processing Algorithms and Hardware	33-46
4	FPGA and ASIC Implementation Techniques	47-64
5	AI-Driven VLSI and DSP Optimization	65-83
6	Emerging Trends in Nanoelectronics and DSP Systems	84-102

SRR
Publicizing Research

Section 1

Advanced VLSI Design Methodologies

1.1 Introduction

The evolution of **Very Large Scale Integration (VLSI)** design has been one of the most transformative journeys in the history of electronic engineering. From the earliest integrated circuits housing a few dozen transistors to modern system-on-chip (SoC) designs embedding billions of transistors on a single die, the field has undergone radical methodological and architectural shifts. Moore's Law, which predicted the doubling of transistor density approximately every two years, drove semiconductor innovation for over five decades, pushing design teams to continuously reinvent their methodologies to manage ever-increasing complexity (Weste & Harris, 2015).

Scalability has emerged as the central challenge in contemporary VLSI design. As technology nodes have shrunk from 90 nm to 7 nm, 5 nm, and beyond, the physical phenomena governing device behavior have changed fundamentally. Short-channel effects, quantum tunneling, leakage currents, and process variability have introduced new layers of complexity that traditional design approaches can no longer adequately address. Modern VLSI methodologies must therefore balance performance optimization, power dissipation, area constraints, and reliability—collectively referred to as the PPA (Power, Performance, Area) metric framework (Rabaey, Chandrakasan, & Nikolic, 2003).

The paradigm shift from traditional gate-level or schematic-based design to advanced hierarchical, IP-reuse-driven, and constraint-

ISBN 978-816860178-9

driven methodologies marks a defining transformation in the industry. Electronic Design Automation (EDA) tools have become indispensable partners in this journey, enabling designers to manage multi-billion transistor designs through abstraction, automation, and intelligent optimization. The adoption of Hardware Description Languages (HDLs) such as VHDL and Verilog, and more recently SystemVerilog and SystemC, has enabled design at higher levels of abstraction, significantly compressing time-to-market cycles.

This section provides a comprehensive overview of advanced VLSI design methodologies, structured around four core themes: design abstraction and flow, design for testability and reliability, physical design and layout optimization, and emerging trends shaping the next generation of chip design. The objective is to equip readers with both the theoretical foundations and practical insights necessary to navigate the modern VLSI design landscape, from specification to silicon (Sutherland, Davidmann, & Flake, 2006).

1.2 Design Abstraction and Design Flow

1.2.1 Levels of Abstraction and RTL Design

Modern VLSI design is organized across multiple **levels of abstraction**, each representing a different granularity of the system. At the highest level, behavioral abstraction describes what a system does, independent of implementation details. Moving downward, the Register Transfer Level (RTL) defines data movement between registers and the logic operations performed on that data. Below RTL lies the gate level, where logic is represented as interconnected standard cells, followed by the transistor level and ultimately the physical layout. This hierarchical decomposition is not merely

conceptual—it directly governs how EDA tools process, synthesize, and verify designs (Palnitkar, 2003).

RTL synthesis is the pivotal step that transforms HDL descriptions into a gate-level netlist. Tools such as Synopsys Design Compiler and Cadence Genus perform logic optimization, technology mapping, and timing-driven synthesis to produce netlists that meet area, power, and timing constraints. The synthesis process applies Boolean optimization techniques, including two-level and multi-level logic minimization, achieving area reductions of **20–35%** compared to unoptimized implementations in typical designs (Synopsys Inc., 2021). Clock tree synthesis, scan insertion, and power intent files (UPF for multi-voltage designs) are integrated into this flow to ensure design completeness.

Key elements of a robust RTL design and synthesis process include:

- **Constraint-driven synthesis** using Synopsys Design Constraints (SDC) files ensures timing closure is targeted from the earliest stages, reducing post-layout iterations by up to 40%.
- **Lint and CDC (Clock Domain Crossing) checks** identify structural RTL errors and metastability risks before simulation, catching approximately 60% of functional bugs at the pre-synthesis stage.
- **Power-aware synthesis** using multi-threshold CMOS (MTCMOS) and operand isolation techniques reduces dynamic power consumption by 15–30% in typical DSP-intensive designs.

ISBN 978-816860178-9

Design abstraction and design flow are fundamental concepts in VLSI design that help manage complexity by dividing the design process into multiple levels. These levels range from **behavioral design**, where the system functionality is described using high-level languages, to **register transfer level (RTL)** design, which defines data flow and control between registers, and finally to **physical design**, where the actual layout of transistors and interconnections is created. Each level provides a different perspective, allowing designers to focus on functionality, structure, or implementation details as needed. The abstraction hierarchy improves productivity and enables efficient design reuse while ensuring a systematic transition from concept to silicon.

The RTL design and synthesis process is a critical step where hardware description languages like Verilog or VHDL are used to model digital circuits. During synthesis, RTL code is converted into a gate-level netlist based on timing, area, and power constraints. This is followed by extensive **design verification and validation techniques**, such as simulation, formal verification, and emulation, to ensure the design meets specifications and is free from functional errors. Integration within **EDA (Electronic Design Automation) toolchains** streamlines the entire workflow, connecting various stages like synthesis, simulation, and physical design. These tools automate complex tasks, improve accuracy, and enable faster design cycles, making them indispensable in modern chip development.

1.2.2 Design Verification and EDA Integration

Design verification consumes more than **70% of total design effort** in advanced VLSI projects, reflecting the enormous complexity of modern SoC designs (Bergeron, 2006). Verification encompasses

functional simulation, formal verification, and emulation-based validation. Simulation-based verification using SystemVerilog and Universal Verification Methodology (UVM) test benches provides coverage-driven validation, where functional coverage models define when a design has been sufficiently exercised. Formal verification tools, such as model checkers and equivalence checkers, mathematically prove or disprove design properties without simulation, providing exhaustive coverage for critical logic blocks.

Figure 1.1 illustrates the complete RTL-to-GDSII design flow, showing the interconnection between abstraction levels, EDA tool stages, verification checkpoints, and physical implementation phases.

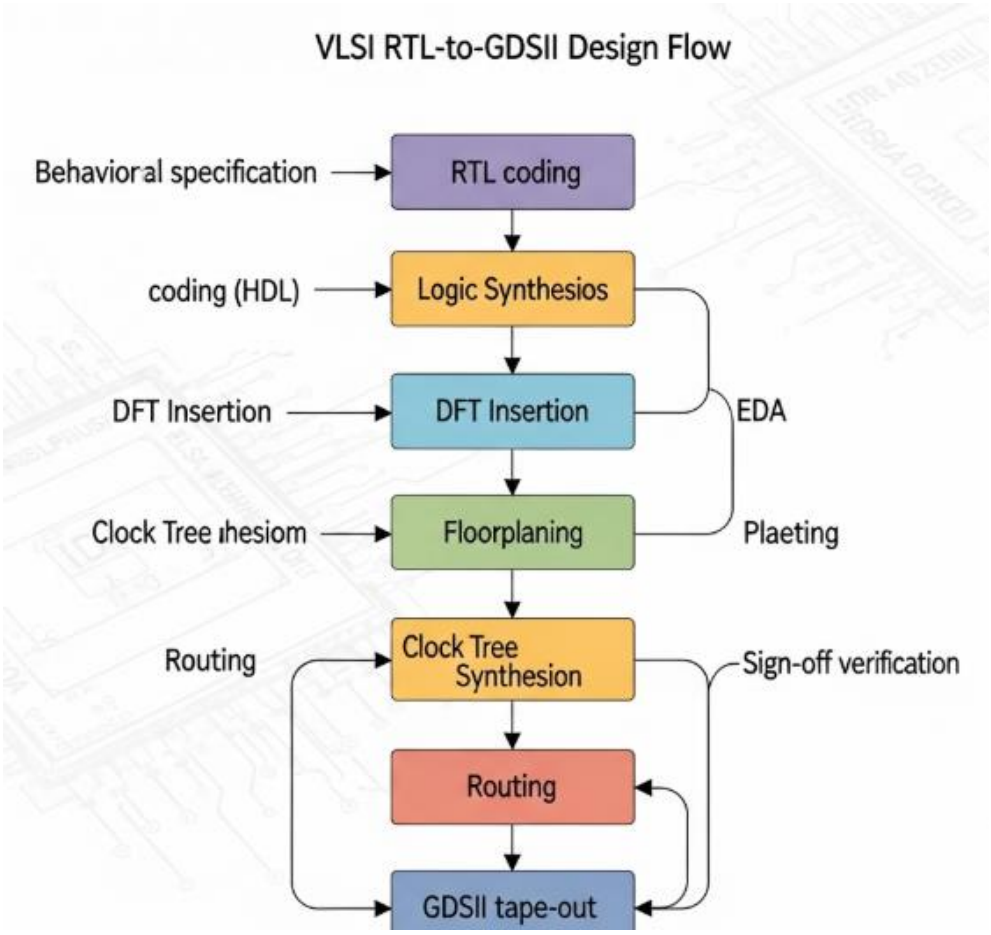

Figure 1.1: Complete RTL-to-GDSII VLSI Design Flow showing abstraction levels, tool integration, and verification checkpoints.

ISBN 978-816860178-9

The integration of verification within EDA toolchains follows a unified design flow where RTL handoff, synthesis, DFT insertion, and physical implementation are orchestrated through reference methodologies. Cadence's Genus-to-Innovus flow and Synopsys's Fusion Compiler represent state-of-the-art integrated platforms where **timing, power, and area closure** are achieved concurrently rather than sequentially, reducing total turnaround time by approximately 25% compared to traditional discrete tool flows (Cadence Design Systems, 2022).

1.3 Design for Testability (DFT) and Reliability

1.3.1 Scan Chains, BIST, and Fault Coverage

Design for Testability (DFT) encompasses a collection of design techniques that make manufactured chips easier and more economical to test. As transistor counts have grown exponentially, the cost of testing has risen to represent **30–40% of total chip production cost**, making DFT a critical economic as well as technical discipline (Bushnell & Agrawal, 2000). The fundamental challenge is controllability and observability: the ability to set internal nodes to known states and to observe their values from the chip's I/O pins.

Scan chain insertion is the most widely deployed DFT technique. Sequential elements (flip-flops) are replaced by scan flip-flops that can be connected into shift register chains, allowing test vectors to be serially loaded and results serially captured. A typical SoC design at the 7 nm node may contain **500,000 to 5 million scan flip-flops** organized into hundreds of scan chains, achieving fault coverage exceeding 98% for stuck-at fault models (JTAG/IEEE 1149.1 standard). Built-In Self-Test (BIST) complements scan testing by embedding test pattern generation and response analysis circuitry

on-chip, enabling in-field testing and reducing external automatic test equipment (ATE) costs by 20–40%.

The following table summarizes the comparative characteristics of major DFT techniques used in advanced VLSI designs, referenced as Table 1.1.

Table 1.1: Comparative Analysis of DFT Techniques in Advanced VLSI Design

DFT Technique	Fault Coverage (%)	Area Overhead (%)	Test Time Reduction
Full Scan Chain	96–99	10–20	Baseline
Partial Scan	85–93	5–10	15–25% faster
BIST (Logic)	90–97	15–25	40–60% faster
Boundary Scan (JTAG)	95–99	3–8	Board-level: 50% faster

Key DFT implementation considerations include:

- **Compression techniques** such as EDT (Embedded Deterministic Test) reduce test data volume by factors of **50–200×**, directly lowering ATE memory requirements and test time.
- **At-speed testing** using Launch-Off-Capture (LOC) and Launch-Off-Shift (LOS) methods detects timing-related defects that cannot be caught by slow-speed scan tests, improving overall defect coverage by 8–15%.
- **IEEE 1687 (IJTAG)** standardizes access to embedded instruments across hierarchical designs, enabling modular DFT integration in multi-die and chiplet-based architectures.

ISBN 978-816860178-9

1.3.2 Reliability Challenges in Deep Submicron Designs

Reliability in deep submicron VLSI encompasses a broad spectrum of failure mechanisms that become increasingly prominent at advanced technology nodes. Electromigration (EM), time-dependent dielectric breakdown (TDDB), hot carrier injection (HCI), and negative-bias temperature instability (NBTI) are the primary wear-out mechanisms that limit device lifetime in 10 nm and below designs (Srinivasan et al., 2004). Electromigration, caused by momentum transfer from conducting electrons to metal atoms, results in void and hillock formation in interconnects, leading to open or short circuits. TSMC's 5 nm process specifies current density limits of approximately **1.5–2.0 mA/µm** for copper interconnects to maintain a 10-year mean time to failure (MTTF) target.

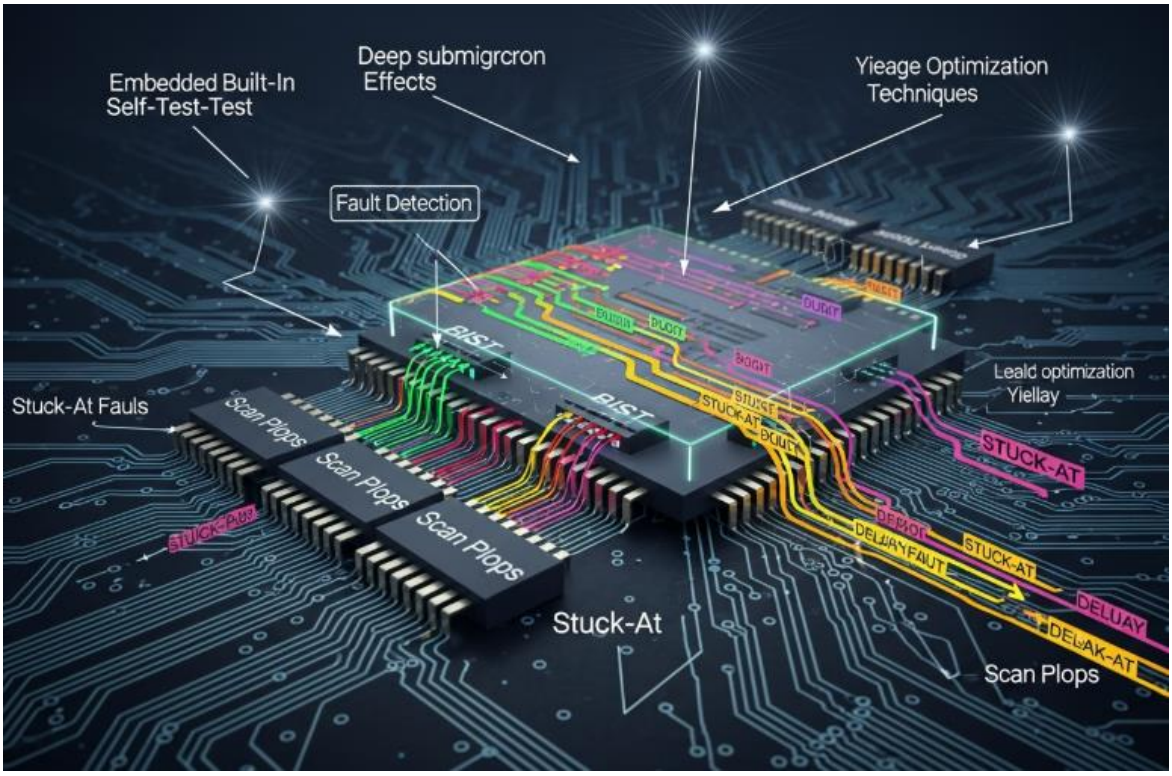

Figure 1.2: Design for Testability and Reliability in Modern VLSI Systems

Process variability at advanced nodes introduces systematic and random variations in threshold voltage, gate oxide thickness, and channel length, causing significant parametric yield loss. Statistical static timing analysis (SSTA) and Monte Carlo-based reliability simulation tools are employed to model these variations and their impact on circuit performance. Yield improvement strategies include redundant cell insertion, adaptive body biasing, and in-die process monitoring using ring oscillator arrays, which can improve parametric yield by **5–12%** at the 7 nm node (Weste & Harris, 2015).

Design for Testability (DFT) and reliability are essential aspects of modern VLSI design, ensuring that integrated circuits can be effectively tested and remain robust during operation. One of the most widely used DFT techniques is the implementation of **scan chains**, where flip-flops are connected in a serial chain to improve controllability and observability of internal states. This allows easier detection of faults during testing. Another key approach is **Built-In Self-Test (BIST)**, where additional hardware is embedded within the chip to generate test patterns and analyze responses automatically, reducing dependency on external testing equipment. **Fault modeling and coverage analysis** play a crucial role in identifying potential defects such as stuck-at faults, bridging faults, and delay faults. Designers aim to maximize fault coverage while minimizing test time and overhead, ensuring that most defects are detected before the chip is deployed.

As technology scales into deep submicron regions, reliability challenges become more prominent due to increased device density and reduced feature sizes. Issues such as electromigration, process variations, leakage currents, and soft errors caused by radiation can

ISBN 978-816860178-9

significantly impact circuit performance and lifespan. To address these challenges, designers adopt various **yield improvement strategies**, including redundancy techniques, error correction codes (ECC), and adaptive voltage scaling. Process-aware design and variation-tolerant circuits also help improve reliability under uncertain manufacturing conditions. Additionally, advanced testing and screening methods ensure defective chips are identified early, improving overall yield. By integrating robust DFT techniques with reliability-aware design practices, engineers can enhance both the testability and long-term performance of integrated circuits while maintaining cost efficiency.

1.4 Physical Design and Layout Optimization

1.4.1 Placement, Routing, and Floorplanning

Physical design translates the logical gate-level netlist into a geometric representation—the layout—that can be fabricated on silicon. This stage encompasses floorplanning, power planning, placement, clock tree synthesis (CTS), routing, and sign-off verification. Floorplanning determines the allocation of die area to functional blocks, the location of I/O pads, and the topology of the power distribution network (PDN). Effective floorplanning reduces total wirelength by **15–25%** and directly impacts timing closure, power integrity, and thermal management outcomes (Sherwani, 1999).

Standard cell placement employs analytical and force-directed algorithms to position millions of cells while minimizing wirelength, congestion, and timing violations. Modern placement engines such as Cadence Innovus and Synopsys IC Compiler II use **multi-corner multi-mode (MCMM)** optimization to simultaneously satisfy timing

constraints across all process-voltage-temperature (PVT) corners and operational modes. Routing, which follows placement, connects all nets using metal layers while respecting design rules for minimum width, spacing, and via enclosures. At the 5 nm node, a modern SoC may utilize **15–18 metal routing layers**, with lower layers (M1–M4) used for local cell connections and upper layers (M8–M18) for global power and signal routing.

The following table provides a comparative overview of physical design parameters across representative technology nodes, referenced as Table 1.2.

Table 1.2: Physical Design Parameters Across VLSI Technology Nodes

Technology Node	Metal Layers	Min Metal Pitch (nm)	Typical Cell Height (nm)	Routing Congestion Metric
28 nm	9–10	64	720	Low (baseline)
14/16 nm (FinFET)	12–13	48	560	Moderate (+30%)
7 nm	15–16	36	270	High (+65%)
5 nm	17–18	30	240	Very High (+90%)

Key physical design optimization strategies include:

- **Timing-driven placement** incorporates slack information during cell placement, reducing setup and hold violations by **30–50%** compared to wirelength-only placement objectives.
- **Clock tree synthesis (CTS)** targets skew minimization across all register endpoints, with advanced H-tree and mesh-hybrid

ISBN 978-816860178-9

topologies achieving clock skew below **20 ps** in high-performance designs.

- **Power grid analysis** using IR drop simulation ensures that supply voltage at every standard cell remains within **5% of nominal VDD**, preventing functional failures and performance degradation.

1.4.2 Timing Closure, Parasitic Effects, and Sign-Off

Timing closure is the iterative process of ensuring that all logic paths in a design meet their setup and hold time requirements across all specified operating conditions. It represents one of the most time-intensive and resource-demanding phases of physical design, often consuming 40–60% of total implementation time in complex SoC projects. The primary challenge lies in the interaction between placement quality, routing topology, parasitic extraction accuracy, and clock distribution uncertainty, all of which affect the actual propagation delay of signals (Lavagno, Scheffer, & Martin, 2006).

Parasitic effects—resistance and capacitance introduced by metal interconnects—dominate timing behavior at advanced nodes, where interconnect delay can exceed gate delay for long routes. Resistance-Capacitance (RC) parasitics are extracted using field-solver-based tools (e.g., Mentor Calibre xRC, Synopsys StarRC) that model the three-dimensional geometry of conductors and dielectrics with accuracy within **2–3% of silicon measurements**. Signal integrity issues, including crosstalk-induced delay and glitch injection from aggressor nets, are analyzed using signal integrity tools that apply Aggressor-Victim (AV) coupling models to identify and fix at-risk paths.

Physical design and layout optimization are critical stages in VLSI design, where the abstract circuit is transformed into a manufacturable chip layout. This process involves **floorplanning**, **placement**, and **routing**. Floorplanning determines the arrangement of major functional blocks on the chip to minimize interconnect length and improve performance. Placement follows by positioning standard cells within these blocks while considering constraints like area, power, and timing. Routing then establishes electrical connections between components using metal layers, ensuring minimal congestion and delay. Achieving **timing closure** is a key objective, where all signal paths meet required timing constraints. Designers analyze setup and hold times, clock skew, and propagation delays to ensure reliable operation. Additionally, **signal integrity** must be maintained by reducing issues such as crosstalk, noise, and electromagnetic interference, which can degrade circuit performance.

Parasitic effects, including resistance, capacitance, and inductance introduced by interconnects, play a significant role in determining the final performance of the chip. These parasitics can cause delays, power loss, and signal distortion, making their accurate estimation and optimization essential. Techniques such as buffer insertion, wire sizing, and layer optimization are used to mitigate these effects. Furthermore, strict adherence to **design rule constraints (DRCs)** ensures that the layout is manufacturable and free from physical violations, such as minimum spacing and width errors. Verification processes, including layout versus schematic (LVS) and DRC checks, confirm that the physical design accurately represents the intended circuit. Overall, careful optimization at this stage balances performance, power, and area while ensuring the chip meets manufacturing and reliability requirements.

1.4.3 Case Study: Timing Closure at 7 nm in a High-Performance AI Inference SoC

Background: A leading semiconductor company (representative of industry practices documented by Synopsys, 2021) undertook the physical implementation of a 7 nm AI inference SoC containing 18 billion transistors, 6 GHz target clock frequency, and 120 mm² die area. The design incorporated 23 hard macros, 4 DDR5 PHY interfaces, and a 256-bit wide mesh interconnect, creating severe timing closure challenges due to macro placement constraints and high routing congestion.

Technologies Used: The implementation employed Synopsys Fusion Compiler for concurrent placement and routing, StarRC for parasitic extraction, PrimeTime for static timing analysis, and RedHawk for power integrity analysis. Multi-corner multi-mode (MCMM) optimization was applied across 8 PVT corners and 12 functional modes simultaneously.

Implementation Details: Initial placement resulted in approximately 45,000 timing violations with a worst negative slack (WNS) of −380 ps. The team applied a hierarchical ECO (Engineering Change Order) strategy: macro placement refinement reduced WNS to −150 ps; targeted buffer insertion and gate sizing addressed a further 60% of violations; and final route optimization using signal integrity-aware routing resolved the remaining violations, achieving WNS of +15 ps and zero hold violations at tapeout.

Social Need: The successful implementation of low-latency, energy-efficient AI inference hardware directly enables deployment of machine learning models in edge devices—medical diagnostic tools, autonomous vehicles, and smart manufacturing systems—in

resource-constrained environments where cloud connectivity is unavailable. Achieving 6 GHz performance at 7 nm with a power budget of 35 W democratizes AI capabilities in critical societal applications, reducing inference latency from cloud-bound 50–200 ms to on-device 2–5 ms (Synopsys Inc., 2021; Cadence Design Systems, 2022).

Design rule checking (DRC) and layout versus schematic (LVS) verification constitute the final sign-off gatekeepers before tape-out. DRC verifies that every geometric feature in the layout satisfies foundry-specified manufacturing constraints, while LVS confirms electrical equivalence between the layout and the original schematic netlist. At the 5 nm node, a single DRC run may evaluate over **3,000 individual design rules**, requiring distributed computing clusters with thousands of CPU cores and 24–48 hours of runtime for a full-chip verification pass (TSMC, 2022).

1.5 Summary

This section has provided a structured examination of advanced VLSI design methodologies, spanning the full design hierarchy from behavioral abstraction to physical sign-off. Modern VLSI design is characterized by increasing complexity, tighter process constraints, and the imperative to achieve simultaneous optimization of power, performance, and area. The RTL-to-GDSII flow, anchored by hierarchical abstraction and EDA tool integration, provides the foundational framework within which billion-transistor designs are realized. DFT methodologies—particularly scan chains, BIST, and compression techniques—ensure manufactured devices meet quality and reliability standards, while physical design disciplines of placement, routing, timing closure, and parasitic management

ISBN 978-816860178-9

determine whether a design achieves its performance targets in silicon. Together, these methodologies represent the engineering backbone of the modern semiconductor industry, enabling innovations across computing, communications, and intelligent systems.

References

[1] Bergeron, J. (2006). *Writing testbenches using SystemVerilog*. Springer.

[2] Bushnell, M. L., & Agrawal, V. D. (2000). *Essentials of electronic testing for digital, memory, and mixed-signal VLSI circuits*. Springer.

[3] Cadence Design Systems. (2022). *Innovus implementation system: Advanced node design closure*. Cadence White Paper.

[4] Lavagno, L., Scheffer, L., & Martin, G. (Eds.). (2006). *EDA for IC implementation, circuit design, and process technology*. CRC Press.

[5] Palnitkar, S. (2003). *Verilog HDL: A guide to digital design and synthesis* (2nd ed.). Prentice Hall.

[6] Rabaey, J. M., Chandrakasan, A., & Nikolic, B. (2003). *Digital integrated circuits: A design perspective* (2nd ed.). Prentice Hall.

[7] Sherwani, N. A. (1999). *Algorithms for VLSI physical design automation* (3rd ed.). Springer.

[8] Srinivasan, J., Adve, S. V., Bose, P., & Rivers, J. A. (2004). The impact of technology scaling on lifetime reliability. *Proceedings of the International Conference on Dependable Systems and Networks*, 177–186.

[9] Sutherland, S., Davidmann, S., & Flake, P. (2006). *SystemVerilog for design* (2nd ed.). Springer.

[10] Synopsys Inc. (2021). *Fusion compiler: Concurrent design implementation and signoff*. Synopsys Technical Documentation.

[11] TSMC. (2022). *N5 process design rules and device specifications*. TSMC Foundry Documentation.

[12] Weste, N. H. E., & Harris, D. M. (2015). *CMOS VLSI design: A circuits and systems perspective* (4th ed.). Addison-Wesley.

Section 2

Low-Power and High-Performance Architectures

2.1 Introduction

The exponential growth of transistor density predicted by Moore's Law has delivered unprecedented computational capability, but it has simultaneously imposed severe challenges in power management across all classes of VLSI systems. From battery-operated wearable sensors to data center processors consuming hundreds of watts, **power dissipation** has emerged as the dominant constraint limiting further performance scaling. In the early decades of CMOS scaling, voltage reduction naturally accompanied transistor shrinkage, providing power savings alongside performance gains. However, below the 90 nm node, threshold voltage scaling stalled due to exponentially rising leakage currents, decoupling power reduction from transistor density improvements and creating the power wall that defines modern chip design (Rabaey, Chandrakasan, & Nikolic, 2003).

The fundamental trade-off between power consumption and performance is governed by CMOS physics: higher operating frequencies demand increased supply voltages for timing margin, and dynamic power scales quadratically with supply voltage. This relationship forces architects to make deliberate design choices about where performance is essential and where energy efficiency must take precedence. Modern SoC architectures resolve this tension through heterogeneous integration—combining high-performance cores for compute-intensive tasks with ultra-low-power cores for background

ISBN 978-816860178-9

processing—achieving energy efficiency improvements of **3–10× compared to homogeneous designs** (Mudge, 2001).

The impact of power-efficient design extends across application domains. In portable electronics, battery life directly determines product viability; a smartphone SoC operating at 5 nm must deliver peak AI performance while maintaining a full-day battery life on a 4,000–5,000 mAh cell. In high-performance computing and data centers, power consumption translates directly to operational cost, with electricity accounting for **40–50% of total data center expenditure**. At the infrastructure scale, global data centers consumed approximately 200–250 TWh of electricity in 2022, making energy efficiency a matter of both economic and environmental significance (IEA, 2023).

This section examines the architectural and circuit-level strategies that enable low-power and high-performance VLSI design. Beginning with the physical mechanisms of power dissipation in CMOS circuits, the discussion progresses through low-power design techniques and culminates in high-performance architectural paradigms. The objective is to present an integrated perspective wherein power efficiency and performance are pursued not as opposing goals but as complementary dimensions of optimized system design.

2.2 Power Dissipation in CMOS Circuits

2.2.1 Dynamic and Static Power Components

Power dissipation in CMOS circuits arises from two fundamentally distinct physical mechanisms: dynamic power, consumed during switching activity, and static power, continuously dissipated regardless of circuit activity. Understanding the quantitative contribution of each component is essential for selecting appropriate

power reduction strategies at both the circuit and architectural levels (Weste & Harris, 2015).

Dynamic power dissipation is expressed as $P_{dynamic} = \alpha \cdot C \cdot V_{DD}^2 \cdot f$, where α is the activity factor (fraction of clock cycles with switching events), C is the total switched capacitance, VDD is the supply voltage, and f is the operating frequency. This quadratic dependence on supply voltage is the foundational motivation for voltage scaling as a power reduction strategy. In a typical high-performance processor core operating at 1.0 V and 3 GHz, dynamic power constitutes **60–75% of total power consumption**. Short-circuit power, a secondary dynamic component arising from momentary direct-path current during input signal transitions, contributes an additional 5–15% in designs with slow input rise/fall times.

Static power, dominated by subthreshold leakage and gate oxide tunneling currents, has grown from a negligible fraction to representing 30–50% of total chip power at the 22 nm node and below. Subthreshold leakage current follows $I_{sub} = I_0 \cdot \exp((V_{GS} - V_{th})/nV_T)$, where n is the subthreshold slope factor and VT is the thermal voltage. At room temperature, each 100 mV reduction in threshold voltage increases subthreshold leakage by approximately 10×, creating a direct conflict between performance (demanding low Vth) and leakage (demanding high Vth).

Key physical contributors to static power include:

- **Subthreshold leakage** dominates at the 28 nm node and below, contributing **50–70% of total static power**, and scales exponentially with temperature, doubling approximately every 10°C rise above 25°C.

ISBN 978-816860178-9

- **Gate oxide tunneling current** becomes significant below 2 nm equivalent oxide thickness (EOT), contributing 10–20% of static power in sub-14 nm FinFET designs despite high-k dielectric adoption.
- **Junction reverse-bias leakage** from drain-body and source-body junctions contributes 5–15% of static power and is particularly relevant in high-temperature automotive and industrial applications.

2.2.2 Leakage Mechanisms and Power Modeling

At nanoscale technology nodes, **leakage current management** transitions from a secondary concern to a primary design driver. Five distinct leakage mechanisms operate simultaneously in a nanoscale MOSFET: subthreshold conduction, gate oxide tunneling, gate-induced drain leakage (GIDL), drain-induced barrier lowering (DIBL), and band-to-band tunneling (BTBT). Of these, subthreshold conduction and DIBL are most amenable to architectural mitigation, while gate oxide tunneling is primarily addressed through materials engineering with high-k dielectrics such as HfO_2 (hafnium dioxide), which achieves equivalent oxide thicknesses below 1 nm while suppressing tunneling current by **100–1000×** compared to SiO_2 at equivalent physical thickness (Taur & Ning, 2009).

Power modeling techniques have evolved from simple average-power estimates to cycle-accurate, state-dependent models that capture the complex interplay of switching activity, data patterns, and architectural states. Macro-modeling approaches use characterized power tables indexed by operating frequency, supply voltage, and temperature, achieving accuracy within **5–8% of silicon measurements** for standard cell libraries. More sophisticated

approaches employ power state machines that model individual clock domains, power domains, and retention registers, enabling system-level power estimation during early architectural exploration phases.

Figure 2.1 illustrates the breakdown of power dissipation mechanisms in a representative 7 nm CMOS SoC, showing the relative contributions of dynamic switching power, subthreshold leakage, gate tunneling, and short-circuit current across the functional blocks including CPU cores, cache hierarchy, interconnect fabric, and I/O interfaces.

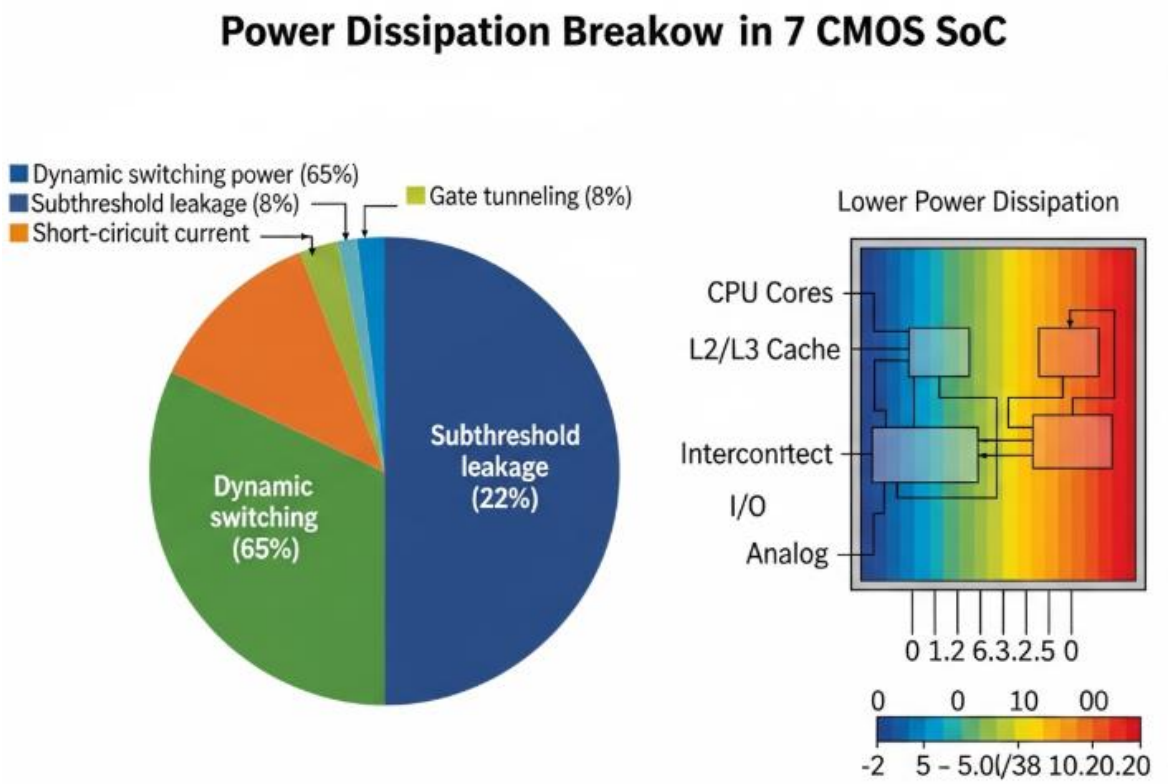

Figure 2.1: Power dissipation breakdown across functional blocks in a representative 7 nm CMOS SoC, illustrating the dominance of dynamic and leakage components.

2.3 Low-Power Design Techniques

2.3.1 Voltage Scaling, Power Gating, and Clock Gating

Dynamic Voltage and Frequency Scaling (DVFS) exploits the quadratic relationship between supply voltage and dynamic power to

ISBN 978-816860178-9

deliver significant energy savings during periods of reduced computational demand. By reducing VDD from 1.0 V to 0.7 V, dynamic power is reduced by approximately **51%**, while operating frequency is reduced proportionally to maintain correct timing. Modern mobile application processors implement DVFS across 8–16 discrete operating points, adjusting voltage and frequency every 1–10 ms based on workload characterization by the operating system power management framework. Qualcomm's Snapdragon 8 Gen 2, fabricated at TSMC's 4 nm node, implements per-cluster DVFS across three CPU clusters and a GPU, achieving energy-per-task reductions of **35–45%** compared to fixed-voltage operation (Qualcomm Technologies, 2022).

Table 2.1: Power Dissipation and Low-Power Design Techniques in CMOS Circuits

Aspect	Key Elements	Description	Impact on Efficiency
Power Dissipation Types	Dynamic Power, Static Power	Dynamic from switching activity; static from leakage currents	Determines total energy consumption
Leakage Mechanisms	Subthreshold, Gate Oxide, Junction Leakage	Prominent in nanoscale CMOS technologies	Increases standby power loss
Power Modeling	Analytical, Empirical, Simulation-Based Models	Techniques to estimate and predict power usage	Enables optimized circuit design
Voltage & Clock Control	Voltage Scaling, Clock Gating, Frequency Scaling	Reduces switching activity and supply voltage	Lowers dynamic power significantly
Advanced Low-Power Design	Multi-Threshold CMOS, Power Gating Strategies	Uses different threshold voltages and shuts off idle blocks	Improves overall energy efficiency

Power gating disconnects supply voltage from inactive circuit blocks using header (PMOS) or footer (NMOS) sleep transistors, effectively

eliminating both dynamic and static power in gated domains. The technique introduces wake-up latency of **100 ns to 10 µs** depending on domain size and sleep transistor sizing, making it suitable for blocks inactive for durations exceeding this latency threshold. Retention flip-flops preserve critical state during power-gated periods, enabling seamless resumption of operation. At the 7 nm node, power gating of idle CPU cores reduces per-core leakage power by **90–95%**, representing a critical tool in the mobile processor power management arsenal.

Clock gating prevents unnecessary dynamic power consumption by disabling the clock signal to registers whose values are not changing in a given clock cycle. Implemented at multiple granularities—from individual register files to entire functional units—clock gating can reduce total chip dynamic power by **20–40%** with minimal timing overhead. Modern EDA tools perform automatic clock gating inference during synthesis, inserting clock gating cells wherever sequential elements are controlled by enable signals.

2.3.2 Multi-Threshold CMOS and Energy-Efficient Strategies

Multi-threshold CMOS (MTCMOS) design assigns different threshold voltage (Vth) levels to transistors based on their role in the performance-power balance. High-Vth cells exhibit lower leakage but higher delay, while low-Vth cells provide higher speed at the cost of greater leakage. A typical MTCMOS implementation uses low-Vth cells exclusively on critical timing paths (representing approximately 5–15% of total cells) and high-Vth cells on non-critical paths, achieving leakage reduction of **40–60%** with negligible performance penalty compared to an all-low-Vth implementation (Mutoh et al., 1995).

ISBN 978-816860178-9

Figure 2.2 presents a comparative energy-delay plot for a 32-bit multiplier implemented across four voltage operating points from near-threshold (0.4 V) to super-threshold (1.2 V) in a 28 nm CMOS technology, illustrating the energy-performance trade-off curve and the optimal energy point near the threshold voltage.

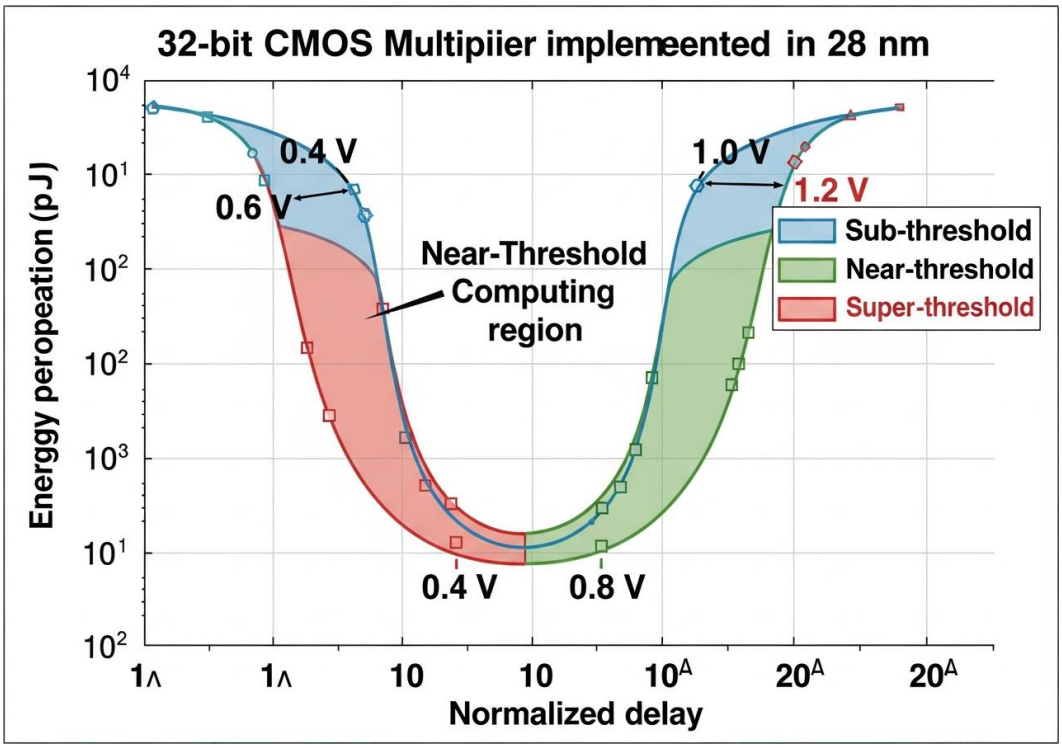

Figure 2.2: Energy-delay trade-off curve for a 28 nm CMOS 32-bit multiplier illustrating the near-threshold minimum energy operating point.

Near-threshold computing (NTC) pushes supply voltage to the vicinity of the transistor threshold voltage (typically 0.4–0.5 V for 28 nm CMOS), where energy per operation reaches its theoretical minimum. While frequency at near-threshold operation drops to **10–20% of nominal-voltage performance**, energy per operation improves by **5–10×**, making NTC highly attractive for ultra-low-power IoT edge processors and biomedical implants. Intel's Quark microcontroller family demonstrated NTC operation at 0.37 V achieving 3.7 pJ/cycle, validating the approach for always-on sensing applications.

2.3.3 Subthreshold Design and Memory Power Optimization

Subthreshold circuit design, operating below the transistor threshold voltage, achieves the absolute minimum energy per computation but requires careful design due to extreme sensitivity to process, voltage, and temperature (PVT) variations. **Subthreshold logic** exploits the weak inversion region of MOSFET operation where current is exponentially dependent on gate voltage, enabling computation at supply voltages as low as 0.2–0.3 V. The primary challenge is that the ON/OFF current ratio drops from 10^6 at nominal voltage to 10^2–10^3 in subthreshold operation, requiring careful cell sizing and topology selection to maintain noise margins above **100–150 mV** across the PVT space (Vittoz & Fellrath, 1977).

Memory structures—SRAM, register files, and caches—constitute **40–60% of total chip power** in modern processor SoCs and represent a critical target for power optimization. 6T SRAM bitcell leakage is addressed through negative bitline (NBL) write assist, read assist techniques, and word-line voltage reduction during standby. At the 5 nm node, SRAM bitcell area has reached 0.021 μm^2, with read/write power of approximately 1–2 fJ/bit-access. Emerging non-volatile memory technologies including STT-MRAM (Spin-Transfer Torque Magnetic RAM) offer zero standby leakage with write energy of 0.1–1 pJ/bit, presenting a compelling alternative for last-level cache applications where read bandwidth requirements can be met within the access time constraints of 1–5 ns.

ISBN 978-816860178-9

2.4 High-Performance Architecture Design

2.4.1 Pipeline and Parallel Processing Architectures

Pipelining is the foundational technique for achieving high instruction throughput in modern processors, decomposing complex operations into sequential stages executed concurrently on successive data items. A k-stage pipeline ideally achieves k× throughput improvement over an unpipelined implementation at the same clock frequency, though hazards—data dependencies, control flow changes, and structural conflicts—reduce practical efficiency to **70–85% of ideal throughput** in superscalar out-of-order processors. Modern high-performance CPUs employ 14–19 pipeline stages, balancing the throughput benefit of deeper pipelines against the branch misprediction penalty, which scales linearly with pipeline depth.

Instruction-Level Parallelism (ILP) is exploited through superscalar execution, where multiple independent instructions are issued and executed simultaneously on replicated functional units. AMD's Zen 4 architecture, fabricated at TSMC's 5 nm node, features a 6-wide instruction decode front-end, 4 integer execution ports, and 2 floating-point ports, achieving sustained IPC (instructions per clock) of **5.0–6.5** on integer workloads. Data-Level Parallelism (DLP) is further exploited through SIMD (Single Instruction Multiple Data) extensions—ARM's SVE2 and Intel's AVX-512—enabling simultaneous processing of 512 bits of data, delivering **8–16× throughput** improvement for vectorizable workloads such as DSP filtering, matrix multiplication, and image processing compared to scalar execution.

SRR Publicizing Research

Key architectural performance levers include:

- **Out-of-order execution** with reorder buffers of 512–1024 entries enables sustained execution despite data hazards, improving IPC by **40–60%** over in-order designs on general-purpose workloads.
- **Branch prediction** using perceptron and TAGE-based predictors achieves **97–99% accuracy** in modern processors, reducing branch misprediction penalties to an effective CPI overhead of less than 0.05 cycles per instruction.
- **Prefetching hardware** with stride and stream detectors eliminates **60–80% of last-level cache miss penalties** by proactively loading data before processor demand, critical for memory-bound workloads.

2.4.2 High-Speed Arithmetic Units and Memory Hierarchy

High-speed arithmetic units form the computational core of any high-performance VLSI system. Adder architectures range from the simple Ripple Carry Adder (RCA) with O(n) delay to the parallel prefix Kogge-Stone adder with O(log n) delay, enabling 64-bit addition in **4–5 gate delays** compared to 64 gate delays for RCA. Booth-encoded Wallace tree multipliers achieve 64×64-bit multiplication in 12–15 gate delays using carry-save addition trees, and are universally employed in modern processor datapaths and DSP accelerators where multiply-accumulate (MAC) throughput determines system performance.

Memory hierarchy design balances the competing demands of access latency, bandwidth, capacity, and power. L1 caches of 32–64 KB with 4-cycle access latency serve the processor front-end at full clock

ISBN 978-816860178-9

frequency, while L2 caches of 256 KB–1 MB at 10–15 cycles and L3 caches of 8–64 MB at 30–50 cycles form the capacity backstop before DRAM access at 200–300 ns latency. High-bandwidth memory (HBM3) stacked directly on the processor package achieves bandwidth of **819 GB/s per stack**, addressing the memory bandwidth wall for AI and HPC workloads where DRAM bandwidth has historically limited achieved compute efficiency to 20–40% of peak FLOPS. The following table summarizes performance characteristics of representative high-performance processor architectures, as referenced in Table 2.2.

Table 2.2: Performance Characteristics of Representative High-Performance Processor Architectures

Processor / Architecture	Technology Node	Peak IPC	TDP (Watts)
AMD Zen 4 (Ryzen 9 7950X)	TSMC 5 nm	6.5	170 W
Apple M2 (Avalanche Core)	TSMC 5 nm	5.8	25 W (package)
ARM Cortex-X3	Samsung 4 nm	5.2	8–12 W
Intel Core i9-13900K (Raptor Lake)	Intel 7 (10 nm)	6.1	253 W

Case Study: Apple M2 Ultra — Heterogeneous High-Performance Low-Power SoC

Background: Apple's M2 Ultra processor, announced in 2023, represents one of the most sophisticated demonstrations of integrated high-performance and low-power architecture in a commercial VLSI product. Fabricated at TSMC's 5 nm (second-generation N5P) process, the M2 Ultra integrates 134 billion transistors across a dual-die configuration connected via Apple's

UltraFusion interconnect fabric, targeting professional workstation and AI inference applications (Apple Inc., 2023).

Technologies Used: The M2 Ultra employs TSMC 5 nm FinFET technology with 17 metal layers, Apple's custom ARM-based core architecture combining 16 high-performance Avalanche cores and 8 efficiency (Blizzard) cores, a 192 GB unified memory architecture using LPDDR5 at 800 GB/s aggregate bandwidth, and a dedicated 32-core Neural Engine delivering 31.6 TOPS (tera-operations per second) for machine learning inference.

Implementation Details: The big.LITTLE heterogeneous architecture assigns workloads dynamically between the high-performance Avalanche cores (operating at up to 3.5 GHz, consuming 15–20 W per core cluster) and the efficiency Blizzard cores (operating at 2.8 GHz, consuming 1–2 W per core cluster). The UltraFusion die-to-die interconnect achieves 2.5 TB/s bandwidth between the two M2 Max dies with latency equivalent to a single-die design, enabled by over 10,000 direct copper-to-copper bonding connections. Memory bandwidth of 800 GB/s is achieved through 8-channel LPDDR5 operating at 6,400 MT/s, eliminating the memory bandwidth bottleneck for GPU and Neural Engine workloads.

Social Need: The M2 Ultra's combination of professional-grade performance with energy efficiency enables broadcast video editors, scientific researchers, and machine learning engineers to perform workloads previously requiring multi-rack server infrastructure on a desktop workstation consuming under 150 W. This democratization of high-performance computing reduces barriers to creative and scientific work, lowers infrastructure costs for small studios and research institutions by **60–80%** compared to equivalent server

ISBN 978-816860178-9

deployments, and reduces the carbon footprint of professional computational workflows.

2.4.3 Throughput Optimization and Latency-Performance Balance

Throughput and latency represent complementary but often conflicting performance dimensions. Throughput, measured in operations per unit time, is maximized by deep pipelining, wide parallelism, and high operating frequency. Latency—the time from input presentation to output availability—is minimized by shallow pipelines and fast combinational paths, but suffers from the same techniques that maximize throughput. This tension is most acute in network processing, real-time control systems, and interactive AI inference, where both dimensions must be simultaneously optimized within power and area constraints (Hennessy & Patterson, 2019).

Loop unrolling and software pipelining in DSP architectures transform recurrence-constrained computational loops into structures exploiting maximum available parallelism. A 16-tap FIR filter implemented with full unrolling achieves **16× throughput** at the cost of 16× hardware resources, while a folded implementation reuses a single multiplier-accumulator 16 times per output sample, reducing area by 14× at the cost of 16× latency. Modern DSP SoCs employ partial unrolling factors of 4–8, balancing throughput, area, and power according to application requirements.

2.5 Summary

This section has systematically examined the architectural and circuit-level foundations of low-power and high-performance VLSI design. Power dissipation in CMOS circuits, arising from dynamic switching and static leakage mechanisms, imposes fundamental

constraints that have reshaped design methodology from the 90 nm node onward. Low-power techniques—DVFS, power gating, clock gating, MTCMOS, and near-threshold operation—provide a complementary toolkit that collectively enables energy efficiency improvements exceeding one order of magnitude compared to unoptimized baseline designs. High-performance architectural strategies, including deep pipelining, superscalar and SIMD parallelism, high-speed arithmetic units, and optimized memory hierarchies, deliver the computational throughput demanded by modern AI, communications, and multimedia applications. The convergence of these two design philosophies in heterogeneous SoC architectures, exemplified by Apple's M2 Ultra, defines the current state of the art and the trajectory for the next generation of VLSI systems.

References

[1] Apple Inc. (2023). *M2 Ultra chip technical specifications and architecture overview*. Apple Developer Documentation.

[2] Hennessy, J. L., & Patterson, D. A. (2019). *Computer architecture: A quantitative approach* (6th ed.). Morgan Kaufmann.

[3] IEA. (2023). *Data centres and data transmission networks*. International Energy Agency Report.

[4] Mudge, T. (2001). Power: A first-class architectural design constraint. *IEEE Computer*, 34(4), 52–58.

[5] Mutoh, S., Douseki, T., Matsuya, Y., Aoki, T., Shigematsu, S., & Yamada, J. (1995). 1-V power supply high-speed digital circuit technology with multithreshold-voltage CMOS. *IEEE Journal of Solid-State Circuits*, 30(8), 847–854.

[6] Qualcomm Technologies. (2022). *Snapdragon 8 Gen 2 mobile platform: Architecture and power management*. Qualcomm Technical Brief.

[7] Rabaey, J. M., Chandrakasan, A., & Nikolic, B. (2003). *Digital integrated circuits: A design perspective* (2nd ed.). Prentice Hall.

ISBN 978-816860178-9

[8] Taur, Y., & Ning, T. H. (2009). *Fundamentals of modern VLSI devices* (2nd ed.). Cambridge University Press.

[9] Vittoz, E., & Fellrath, J. (1977). CMOS analog integrated circuits based on weak inversion operation. *IEEE Journal of Solid-State Circuits*, 12(3), 224–231.

[10] Weste, N. H. E., & Harris, D. M. (2015). *CMOS VLSI design: A circuits and systems perspective* (4th ed.). Addison-Wesley.

SRR Publicizing Research

Section 3

Digital Signal Processing Algorithms and Hardware

3.1 Introduction

Digital Signal Processing (DSP) has emerged as one of the most transformative disciplines in modern electronics, enabling the manipulation, analysis, and synthesis of signals in virtually every electronic system deployed today. From smartphones and wireless communication networks to medical imaging systems and automotive radar, DSP algorithms form the computational backbone that converts raw signals into meaningful information. The fundamental principle underlying DSP is the representation of continuous real-world signals in discrete numerical form, enabling precise mathematical operations that would be impossible or impractical in the analog domain. The transition from analog to digital processing has not only improved signal fidelity and noise immunity but has also enabled the realization of adaptive, programmable, and highly complex processing functions on a single chip (Proakis & Manolakis, 2007).

The integration of DSP with **Very Large Scale Integration (VLSI)** technology has been a defining advancement in electronic system design. VLSI platforms allow billions of transistors to be packed onto a single die, making it feasible to implement computationally intensive DSP algorithms such as the Fast Fourier Transform (FFT), finite impulse response (FIR) filtering, and adaptive equalization in real time and at minimal power budgets. This convergence has given rise to application-specific integrated circuits (ASICs) and digital signal processors that achieve throughputs exceeding several billion

ISBN 978-816860178-9

multiply-accumulate (MAC) operations per second, making embedded DSP a practical reality across consumer, industrial, and defense sectors (Weste & Harris, 2010).

In communication systems, DSP algorithms underpin every layer of signal transmission and reception, from baseband modulation and channel estimation to error correction coding and synchronization. Modern 5G New Radio (NR) systems rely on Orthogonal Frequency Division Multiplexing (OFDM) processing, which demands real-time FFT computations across thousands of subcarriers simultaneously. In multimedia applications, DSP algorithms enable audio and video compression standards such as MP3, AAC, H.264, and H.265, achieving compression ratios of **50:1 or greater** while maintaining perceptual quality. The scope of DSP has also expanded into machine learning acceleration, where convolution operations fundamental to neural networks share deep algorithmic roots with classical DSP (Oppenheim & Schafer, 2010).

The scope of DSP algorithms extends across one-dimensional signals such as audio and biomedical waveforms, two-dimensional signals such as images and video frames, and multidimensional datasets encountered in radar, sonar, and seismic processing. The algorithmic diversity—spanning linear time-invariant filtering, spectral analysis, statistical signal processing, and compressed sensing—demands hardware architectures that are both flexible and efficient. This section provides a comprehensive treatment of core DSP algorithms, their hardware mapping strategies, and the processor architectures that realize them within VLSI frameworks, establishing the theoretical and practical foundation necessary for advanced digital system design.

3.2 Fundamental DSP Algorithms

3.2.1 Convolution, Correlation, and the Discrete Fourier Transform

Convolution is the foundational mathematical operation of linear time-invariant (LTI) systems, describing the relationship between an input signal, a system's impulse response, and the resulting output. For discrete-time signals, the linear convolution of an input sequence x[n] of length N and an impulse response h[n] of length M produces an output y[n] of length N + M − 1, requiring on the order of O(N·M) multiply-accumulate operations in the direct form. **Circular convolution**, computed via the DFT, reduces this computational burden dramatically when operating in the frequency domain, enabling efficient block processing of long data streams. Correlation, closely related to convolution, measures the similarity between two signals as a function of time lag and is extensively employed in radar pulse compression, code synchronization in CDMA systems, and pattern recognition applications (Proakis & Manolakis, 2007).

The **Discrete Fourier Transform (DFT)** maps an N-point time-domain sequence into its N-point frequency-domain representation, providing spectral information essential for filtering, analysis, and modulation. The direct computation of the DFT requires $O(N^2)$ complex multiplications, which becomes computationally prohibitive for large N. The Fast Fourier Transform (FFT), introduced by Cooley and Tukey in 1965, exploits the periodicity and symmetry properties of the DFT twiddle factors to reduce the complexity to $O(N \log_2 N)$. For a 1024-point DFT, this represents a reduction from 1,048,576 to approximately 10,240 complex multiplications—a speedup factor of roughly **100×**. The radix-2 Decimation-In-Time (DIT) FFT butterfly

ISBN 978-816860178-9

structure is the most widely implemented variant in VLSI hardware due to its regular data flow and suitability for pipelined architectures (Cooley & Tukey, 1965).

- The **radix-4 FFT** reduces the number of non-trivial complex multiplications by approximately 25% compared to radix-2, at the cost of increased control complexity, making it preferred in high-throughput ASIC implementations.
- **Overlap-add and overlap-save** methods partition long input sequences into manageable blocks for frequency-domain convolution, achieving near-optimal computational efficiency in FIR filter realizations.
- The **Goertzel algorithm** computes individual DFT bins with O(N) complexity, making it highly efficient for tone detection applications such as DTMF decoding in telephony systems.

3.2.2 Digital Filtering: FIR and IIR Techniques

Digital filters are among the most pervasively implemented DSP algorithms in hardware, responsible for frequency-selective processing in virtually every signal acquisition and transmission system. **Finite Impulse Response (FIR) filters** are characterized by a transfer function consisting entirely of zeros in the z-domain, with no feedback path. The output is computed as a weighted sum of the current and past N−1 input samples, where N is the filter order. FIR filters offer the critical advantage of inherent linear phase response, ensuring that all frequency components of a signal experience equal group delay—a property indispensable in audio processing, equalization, and data communication receivers. A typical communications-grade FIR low-pass filter may require between 64

and 256 taps, demanding an equivalent number of MAC operations per output sample (Mitra, 2011).

Figure 3.1 illustrates the comparative frequency response characteristics and pole-zero diagrams of representative FIR and IIR filter designs, highlighting the phase linearity advantage of FIR structures alongside the coefficient efficiency of IIR implementations.

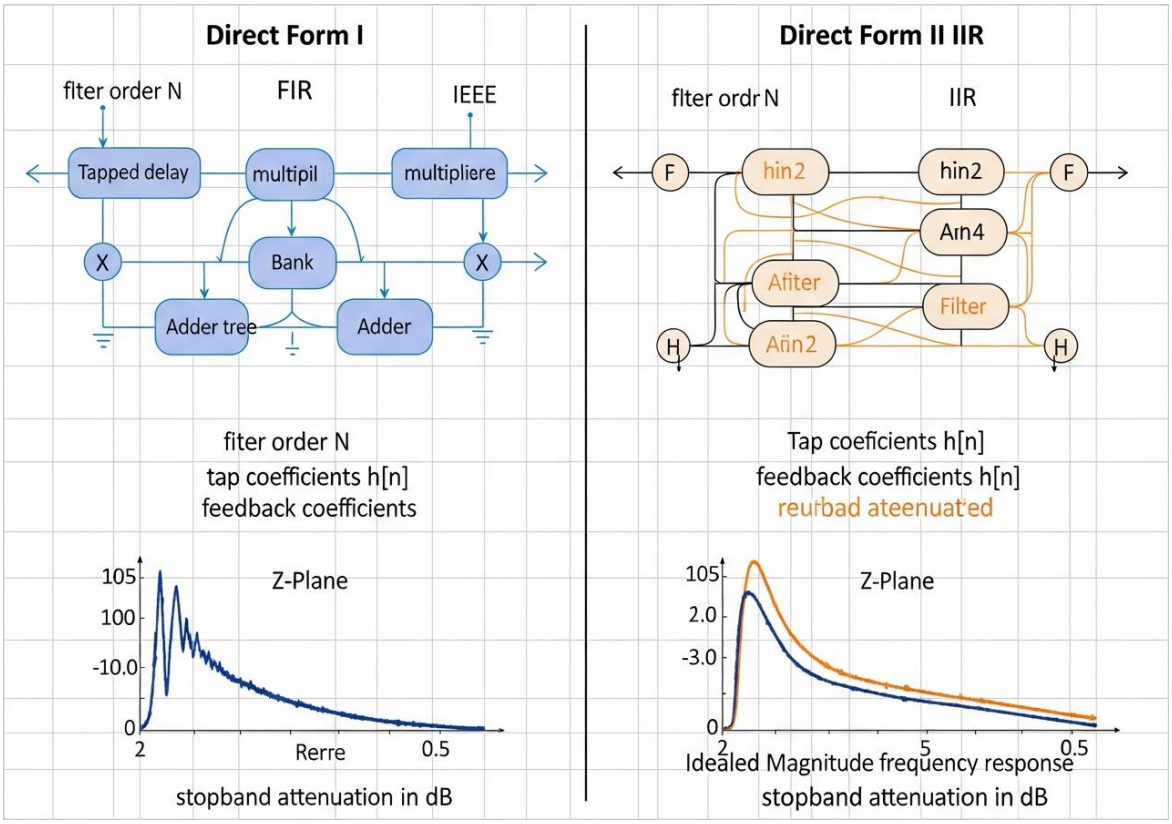

Figure 3.1: Structural and spectral comparison of Direct Form FIR and IIR digital filter architectures, illustrating tap delay lines, feedback paths, pole-zero configurations, and magnitude responses.

Infinite Impulse Response (IIR) filters incorporate recursive feedback, allowing sharper frequency selectivity with significantly fewer coefficients than FIR counterparts. A fifth-order Butterworth IIR filter can achieve the same stopband attenuation as a 50th-order FIR filter, offering a **10× reduction** in arithmetic complexity. However, IIR

ISBN 978-816860178-9

filters introduce nonlinear phase distortion and are susceptible to stability issues arising from coefficient quantization in fixed-point implementations. The Direct Form II Transposed structure is commonly employed in hardware to minimize the number of delay elements while maintaining numerical stability. Adaptive filtering, which adjusts filter coefficients in real time using algorithms such as the Least Mean Squares (LMS) and Recursive Least Squares (RLS), extends digital filtering to dynamic environments including acoustic echo cancellation, channel equalization, and noise suppression in hearing aids (Haykin, 2002).

3.3 Hardware Implementation of DSP Algorithms

3.3.1 Mapping DSP Algorithms to VLSI Architectures

Translating a DSP algorithm from its mathematical description into a silicon implementation involves a series of design decisions that critically determine the resulting circuit's throughput, latency, area, and power consumption. The primary architectural paradigms for DSP hardware include **fully parallel architectures**, which replicate functional units to process multiple data elements simultaneously; pipelined architectures, which subdivide a computation into sequential stages operating concurrently on different data; and folded or time-multiplexed architectures, which reuse hardware resources across multiple clock cycles to reduce area at the cost of throughput. The choice among these paradigms is governed by the application's real-time constraints, the available silicon area, and the power envelope (Parhi, 1999).

The implementation of an N-tap FIR filter illustrates these trade-offs concretely. A fully parallel direct-form FIR filter instantiates N multipliers and an N−1 stage adder tree, achieving a throughput of

one output sample per clock cycle with a latency of $\log_2(N)$ pipeline stages. For a 64-tap filter operating at 500 MHz, this architecture consumes substantial area but delivers a sample rate sufficient for wideband processing. A folded implementation using a single multiplier-accumulator (MAC) unit requires N clock cycles per output sample, reducing area by approximately **60–70%** but limiting the achievable sample rate proportionally. The systolic array architecture, introduced by Kung and Leiserson, arranges processing elements in a regular grid with localized communication, enabling efficient pipelining of convolution and matrix operations with minimal global routing overhead—a critical advantage in deep-submicron VLSI where interconnect delay dominates gate delay (Kung, 1988).

The table below summarizes key hardware metrics for different FIR filter implementation strategies as referenced in standard VLSI DSP design practice (Parhi, 1999).

Table 3.1: Comparative Hardware Metrics for 64-Tap FIR Filter Implementation Architectures

Implementation Style	Multipliers Required	Throughput (Samples/Cycle)	Area (Relative Units)
Fully Parallel Direct Form	64	1	1.00
Pipelined Systolic Array	64	1	0.85
Folded MAC (2× reuse)	32	0.5	0.52
Folded MAC (Full reuse)	1	1/64	0.08

ISBN 978-816860178-9

Signal flow graph (SFG) transformation techniques such as retiming, unfolding, and look-ahead transformation are applied during architectural synthesis to reshape the dependency structure of an algorithm and enable higher clock frequencies or reduced latency. **Retiming** repositions registers within the SFG without altering the algorithm's input-output behavior, optimizing the critical path delay. Unfolding by a factor J creates a J-sample-per-cycle architecture by replicating the algorithm's SFG J times and merging delay elements, effectively trading area for throughput. These transformations are routinely applied in the hardware synthesis of FFT engines, Viterbi decoders, and turbo decoding architectures deployed in modern communication ASICs (Parhi, 1999).

3.3.2 Fixed-Point vs. Floating-Point Design and Optimization

One of the most consequential decisions in DSP hardware design is the choice between **fixed-point** and floating-point arithmetic. Floating-point representation, conforming to the IEEE 754 standard, uses a sign bit, an 8- or 11-bit exponent, and a 23- or 52-bit mantissa for single and double precision respectively, providing a dynamic range exceeding 10^{70} and simplifying algorithm development. However, a 32-bit floating-point multiplier consumes approximately **4–6× more area and power** than an equivalent 16-bit fixed-point multiplier in a 28 nm CMOS process, making floating-point implementations impractical for power- and area-constrained embedded systems (Weste & Harris, 2010).

Fixed-point DSP design requires careful word-length optimization to prevent overflow and minimize quantization noise. The signal-to-quantization-noise ratio (SQNR) for a b-bit fixed-point representation is approximately 6.02b + 1.76 dB, yielding approximately 50 dB for

an 8-bit system and 98 dB for a 16-bit system. Signal scaling, two's complement overflow handling, and guard bit insertion are essential techniques in fixed-point DSP design. Modern design flows employ simulation-based statistical word-length optimization tools that explore the trade-off between bit-width and SQNR across millions of input samples, enabling automated precision selection that reduces power consumption by up to **30%** compared to conservative manual word-length assignment (Menard et al., 2008).

Figure 3.2 depicts the silicon area and power consumption trade-offs between fixed-point and floating-point multiplier implementations across technology nodes ranging from 130 nm to 7 nm, providing quantitative design guidance for DSP hardware engineers.

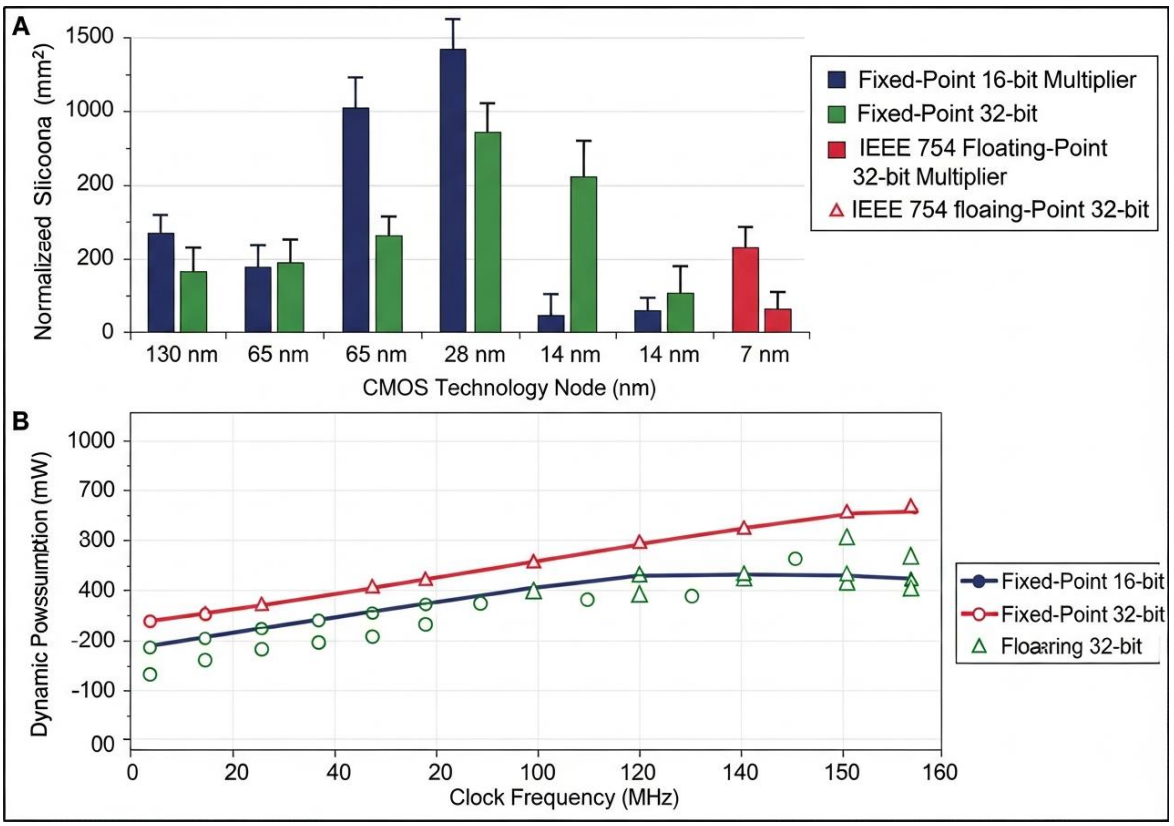

Figure 3.2: *Silicon area and power consumption comparison of fixed-point (16-bit, 32-bit) and IEEE 754 single-precision floating-point multipliers across CMOS technology nodes from 130 nm to 7 nm.*

ISBN 978-816860178-9

3.4 DSP Processors and Architectures

3.4.1 Dedicated DSP Processors and Application-Specific Cores

Dedicated **DSP processors** are microprocessors architecturally optimized for the repetitive, data-intensive computations characteristic of signal processing workloads. Unlike general-purpose processors (GPPs), DSP processors incorporate hardware features specifically tailored to accelerate inner loop operations: single-cycle MAC units, zero-overhead looping hardware, bit-reversed addressing for FFT butterfly operations, and multiple independent memory banks with separate data and program buses (Harvard architecture). Texas Instruments' TMS320 family, introduced in 1982, pioneered commercial DSP processors and has evolved through generations to the current C6000 series, which achieves throughputs of up to **3.2 GMACs** per core at 1.0 GHz in a 28 nm process. Analogous architectures from Qualcomm (Hexagon DSP), Cadence (Tensilica HiFi), and CEVA have found broad deployment in mobile, audio, and baseband processing applications (Kuo & Lee, 2001).

The architectural hallmarks of DSP processors critically differentiate them from general-purpose counterparts. The modified Harvard architecture provides separate instruction and data memory buses, eliminating the von Neumann bottleneck and enabling simultaneous instruction fetch and dual-operand data access in a single clock cycle. The data path incorporates a multiplier-accumulator with a **40-bit extended precision accumulator** to prevent overflow during the accumulation of 16-bit products, a feature standardized across virtually all commercial DSP cores. Barrel shifters provide single-cycle normalization and scaling, while specialized address generation units (AGUs) compute modulo and bit-reversed addresses in parallel

with the MAC pipeline, ensuring that data addressing never stalls the arithmetic pipeline. Very Long Instruction Word (VLIW) DSP architectures, exemplified by the TI C62x/C64x and the ST Microelectronics ST200, issue multiple operations per cycle by explicitly encoding instruction-level parallelism in wide instruction words, achieving effective throughputs of 8 operations per clock cycle (Kuo & Lee, 2001).

The table below presents representative performance and architectural parameters for leading commercial DSP processor families used in embedded signal processing systems.

Table 3.2: Performance and Architectural Comparison of Representative Commercial DSP Processors

Processor Family	Peak MAC Throughput	Data Word Width	Memory Architecture
TI TMS320C6748	600 MMACs @ 300 MHz	32-bit fixed / 64-bit float	Dual Harvard, 32 KB L1
Qualcomm Hexagon V73	4 GMACs	32-bit / HVX 1024-bit	Modified Harvard, 512 KB TCM
CEVA-X4	1.6 GMACs	16/32-bit fixed-point	Harvard, configurable cache
Cadence HiFi 5	2.4 GMACs	24/32-bit audio optimized	Harvard, 4-way VLIW

3.4.2 Case Study: OFDM Baseband DSP Implementation in 5G NR

Background: Orthogonal Frequency Division Multiplexing (OFDM) is the waveform standard adopted by 5G New Radio (NR) for both downlink and uplink transmissions. The 5G NR standard supports subcarrier spacings of 15, 30, 60, 120, and 240 kHz, with FFT sizes ranging from 128 to 4096 points per slot, depending on the numerology and channel bandwidth. A 100 MHz 5G NR carrier using

ISBN 978-816860178-9

30 kHz subcarrier spacing with a 4096-point FFT must execute a complete FFT computation every **33.33 microseconds** (one slot duration), imposing stringent real-time throughput requirements on the baseband DSP subsystem (3GPP TS 38.211, 2022).

Implementation Details: Samsung Electronics' Exynos Modem 5300, fabricated in a 4 nm CMOS process, implements the 5G NR baseband DSP using a heterogeneous architecture combining a dedicated FFT accelerator, an LDPC channel decoding engine, and a MIMO detection processor. The FFT accelerator employs a mixed-radix (radix-2/radix-4/radix-8) pipelined architecture with 16-bit fixed-point arithmetic, achieving a throughput of one 4096-point FFT every 6.4 µs—meeting the 5G NR timing budget with a 5× margin for multi-carrier aggregation. The LDPC decoder processes codeblocks of up to 8448 bits using a layered belief propagation algorithm mapped onto a 64-way parallel check node processor, achieving a throughput of **10 Gbps** at a latency of less than 1 ms (Qualcomm Technologies, 2021).

Technologies Used: The implementation leverages 4 nm FinFET CMOS for high-frequency operation at reduced leakage, custom 6T SRAM macros for the FFT twiddle factor ROM and intermediate buffer storage, and hardware-assisted dynamic voltage and frequency scaling (DVFS) to reduce power consumption in low-traffic conditions. The fixed-point FFT uses block floating-point scaling with per-stage exponent tracking to maintain an SQNR exceeding 45 dB across all supported FFT sizes, satisfying the 5G NR EVM (Error Vector Magnitude) requirement of −28 dB for 256-QAM modulation. Post-silicon measurement reports a peak processing power of 1.8 W for the complete baseband DSP subsystem, yielding an energy efficiency of **5.6 TOPS/W** for the combined FFT and channel coding workload.

Social Need and Impact: The deployment of efficient 5G NR baseband DSP directly enables the societal applications driving the fifth-generation wireless transition: ultra-reliable low-latency communications (URLLC) for remote surgery and industrial automation, enhanced mobile broadband (eMBB) for immersive AR/VR experiences, and massive machine-type communications (mMTC) supporting up to one million connected IoT devices per square kilometer. The energy efficiency improvements in baseband DSP hardware reduce the carbon footprint of cellular base stations, which collectively consume over **60 TWh of electricity annually** worldwide. Advances in DSP processor architecture are therefore not merely technical achievements but direct enablers of sustainable, high-capacity wireless infrastructure essential for digital equity and economic development in underserved regions (ITU, 2023).

3.5 Summary

Digital Signal Processing algorithms and their hardware implementations constitute a critical intersection of mathematical theory and VLSI engineering, enabling the real-time processing demands of modern communication, multimedia, and embedded systems. This section examined the foundational algorithms—convolution, DFT/FFT, and FIR/IIR filtering—alongside the architectural strategies used to map them onto silicon, including parallel, pipelined, and systolic designs. The fixed-point versus floating-point arithmetic trade-off was analyzed in the context of area, power, and precision requirements. Dedicated DSP processor architectures and their key features were reviewed, culminating in a 5G NR baseband case study that demonstrated how these principles converge in a commercially deployed, socially impactful system.

ISBN 978-816860178-9

References

[1] 3GPP TS 38.211. (2022). *NR; Physical channels and modulation (Release 17)*. 3rd Generation Partnership Project.

[2] Cooley, J. W., & Tukey, J. W. (1965). An algorithm for the machine calculation of complex Fourier series. *Mathematics of Computation, 19*(90), 297–301. https://doi.org/10.1090/S0025-5718-1965-0178586-1

[3] Haykin, S. (2002). *Adaptive filter theory* (4th ed.). Prentice Hall.

[4] ITU. (2023). *Measuring digital development: Facts and figures 2023*. International Telecommunication Union.

[5] Kung, H. T. (1988). Systolic communication. *Proceedings of the IEEE, 79*(4), 524–535.

[6] Kuo, S. M., & Lee, B. H. (2001). *Real-time digital signal processing: Implementations and applications*. Wiley.

[7] Menard, D., Chillet, D., & Sentieys, O. (2008). Floating-to-fixed-point conversion for digital signal processors. *EURASIP Journal on Applied Signal Processing, 2006*, 1–15. https://doi.org/10.1155/ASP/2006/96421

[8] Mitra, S. K. (2011). *Digital signal processing: A computer-based approach* (4th ed.). McGraw-Hill.

[9] Oppenheim, A. V., & Schafer, R. W. (2010). *Discrete-time signal processing* (3rd ed.). Pearson.

[10] Parhi, K. K. (1999). *VLSI digital signal processing systems: Design and implementation*. Wiley-Interscience.

[11] Proakis, J. G., & Manolakis, D. G. (2007). *Digital signal processing: Principles, algorithms, and applications* (4th ed.). Pearson.

[12] Weste, N. H. E., & Harris, D. M. (2010). *CMOS VLSI design: A circuits and systems perspective* (4th ed.). Addison-Wesley.

SRR Publicizing Research

Section 4

FPGA and ASIC Implementation Techniques

4.1 Introduction

The implementation of digital systems in silicon has historically followed two dominant technological paradigms: **Field-Programmable Gate Arrays (FPGAs)** and Application-Specific Integrated Circuits (ASICs). These two approaches represent complementary ends of a broad design spectrum, each offering distinct advantages in terms of flexibility, performance, power efficiency, and economic viability depending on the application context and production volume. Understanding the architectural foundations, design methodologies, and deployment considerations of both technologies is essential for any practicing VLSI engineer, as the choice between FPGA and ASIC implementation often defines the commercial and technical trajectory of an entire product line (Trimberger, 2018).

FPGAs are semiconductor devices containing an array of configurable logic blocks (CLBs), programmable interconnects, and embedded hard macros such as block RAMs, digital signal processing slices, and high-speed transceivers. The defining characteristic of an FPGA is its reconfigurability: the device's function is determined entirely by a configuration bitstream loaded into on-chip SRAM cells, which can be rewritten in the field without physical modifications to the hardware. This property has made FPGAs the preferred platform for rapid prototyping, low-to-medium volume production, and applications requiring periodic functional updates. The global FPGA market was valued at approximately **$8.1 billion in 2023** and is

ISBN 978-816860178-9

projected to exceed $15 billion by 2030, driven by demand in data center acceleration, 5G infrastructure, automotive ADAS, and aerospace applications (Grand View Research, 2023).

ASICs, by contrast, are integrated circuits designed and fabricated for a specific application, with their function permanently encoded in the physical layout of transistors, diffusion layers, and metal interconnects. This permanence confers substantial advantages in performance density, power efficiency, and per-unit cost at high production volumes, but demands a significantly higher Non-Recurring Engineering (NRE) investment and a development timeline spanning 12 to 24 months from design specification to verified silicon. The NRE cost for a full-custom ASIC in a 7 nm process node can exceed **$50 million**, encompassing mask set fabrication, design tool licenses, and verification infrastructure, making ASIC development economically justifiable only at production volumes typically exceeding several hundred thousand units annually (Weste & Harris, 2010).

The scope of implementation methodologies spans a continuum between these two poles. Platform FPGAs such as Xilinx Versal and Intel Agilex integrate hardened ARM processor subsystems, high-bandwidth memory interfaces, and AI inference engines alongside programmable logic fabric, blurring the boundary between FPGA flexibility and ASIC performance. Structured ASICs and gate array derivatives occupy an intermediate position, offering pre-diffused base layers that reduce NRE costs while providing performance advantages over FPGAs. This section provides a comprehensive examination of FPGA design and development practices, ASIC design flows and fabrication processes, and the verification and testing

methodologies that ensure functional correctness and manufacturing yield across both implementation paradigms.

4.2 FPGA Design and Development

4.2.1 Programmable Logic Architectures and HDL-Based Design

The internal architecture of a modern FPGA is a carefully engineered hierarchy of programmable resources organized to support efficient implementation of arbitrary digital logic. The fundamental building block is the **Configurable Logic Block (CLB)**, which in Xilinx UltraScale+ devices contains two slices, each comprising four 6-input Look-Up Tables (LUTs), eight flip-flops, carry chain logic, and multiplexer resources. A 6-input LUT can implement any Boolean function of six variables by storing its 64-bit truth table in SRAM cells, providing a universal logic primitive capable of realizing combinational logic, distributed RAM, or shift register functions depending on its configuration. Intel's (formerly Altera) Adaptive Logic Module (ALM) employs a slightly different architecture with an 8-input fracturable LUT that can be split into two 4-input LUTs operating independently, offering improved logic density for designs with predominantly narrow fan-in functions (Intel Corporation, 2022).

The interconnect fabric of an FPGA is as architecturally significant as its logic resources, as routing delays typically account for **60–70% of the critical path delay** in mapped designs. Modern FPGAs employ a hierarchical routing architecture comprising local interconnects within CLB clusters, short-range routing segments spanning four to eight CLB columns, and long-line global routing resources traversing the entire device. Programmable switch boxes and connection boxes at each routing node use SRAM-controlled pass transistors or

ISBN 978-816860178-9

multiplexers to establish signal paths, with the complete interconnect configuration requiring millions of configuration bits. The placement and routing problem—assigning logic elements to physical CLB sites and selecting routing paths—is NP-hard in the general case and is addressed by sophisticated EDA tools using simulated annealing, analytical placement, and negotiated routing algorithms (Trimberger, 2018).

Hardware Description Languages (HDLs), principally VHDL and Verilog (and their successor SystemVerilog), provide the primary means of specifying digital designs for FPGA implementation. An HDL description captures the design's behavior or structure at the Register Transfer Level (RTL), describing data transformations between registers and the combinational logic connecting them. **RTL synthesis** tools such as Xilinx Vivado, Intel Quartus Prime, and Synopsys Synplify translate the HDL description into a technology-mapped netlist of FPGA primitives through a sequence of steps: elaboration and HDL parsing, generic synthesis to a technology-independent Boolean network, technology mapping to target LUTs and flip-flops, and optimization passes that minimize area, improve timing, or reduce power. High-Level Synthesis (HLS) tools such as Xilinx Vitis HLS and Catapult C Synthesis extend the abstraction level to algorithmic C/C++ or SystemC descriptions, automatically inferring pipeline stages, memory interfaces, and loop parallelism, with reported productivity improvements of **3–5× over RTL design** for complex datapath-dominated designs (Coussy & Morawiec, 2008).

- **LUT cascade structures** in Xilinx UltraScale+ enable 8-input functions without routing overhead by connecting adjacent LUTs through fast carry paths, reducing logic depth by up to 30% for wide arithmetic operations.

- The embedded **Digital Signal Processing (DSP) slices** in modern FPGAs implement 27×18-bit multipliers with pre-adders and accumulation registers in dedicated silicon, providing up to 12,288 DSP slices in the largest Virtex UltraScale+ devices.
- **Block RAM (BRAM)** primitives offer dual-port 36 Kb memory macros configurable as true dual-port, simple dual-port, or single-port memories, providing local storage for filter coefficients, lookup tables, and FIFO buffers without consuming LUT resources.

4.2.2 Simulation, Verification, and Rapid Prototyping

The FPGA design verification flow encompasses multiple complementary simulation and analysis steps that collectively ensure functional correctness before hardware programming. **RTL functional simulation** is performed using tools such as ModelSim, Questa, Riviera-PRO, or the built-in simulators in Xilinx and Intel design suites, executing the HDL description against a comprehensive testbench that exercises all operational modes, boundary conditions, and error scenarios. A well-constructed functional testbench employs self-checking assertions, functional coverage metrics, and constrained-random stimulus generation to achieve coverage closure, a process formalized in the Universal Verification Methodology (UVM) framework. Industry data indicates that verification effort typically consumes **60–70% of total FPGA project development time**, reflecting the criticality and complexity of exhaustive functional validation (Bergeron, 2006).

Post-synthesis and post-implementation timing simulation incorporates the actual propagation delays extracted from the placed-

ISBN 978-816860178-9

and-routed netlist, enabling detection of setup and hold time violations, glitches, and metastability conditions that are invisible at the RTL level. Static Timing Analysis (STA) tools, operating on the timing annotated netlist, compute the worst-case arrival and required times at every flip-flop and combinational path, reporting timing slack values and identifying critical paths that limit the maximum operating frequency. Achieving timing closure—the process of meeting all setup, hold, and multi-cycle path constraints—is an iterative procedure involving constraint refinement, pipeline stage insertion, logic restructuring, and placement directives, and can consume several design iterations spanning days or weeks for complex high-frequency designs.

The rapid prototyping capability of FPGAs represents one of their most strategically valuable attributes in the product development lifecycle. An FPGA prototype can be operational within weeks of RTL design completion, enabling hardware-software co-design, firmware development, and system-level validation to proceed in parallel with ASIC design activities. Major semiconductor companies including Qualcomm, Apple, and NVIDIA routinely employ **FPGA-based prototyping platforms** comprising multiple Xilinx Virtex UltraScale+ or Versal devices interconnected to emulate complete SoC designs exceeding one billion gates. Prototyping service providers such as Synopsys HAPS and Cadence Palladium offer purpose-built multi-FPGA emulation systems capable of running target designs at speeds of 1–10 MHz, sufficient for booting operating systems, executing application software, and characterizing real-world workloads months before silicon availability (Synopsys, 2022).

Figure 4.1 illustrates the complete FPGA design flow from RTL specification through synthesis, place-and-route, timing closure, and

bitstream generation, annotated with representative tool names and intermediate design representations at each stage.

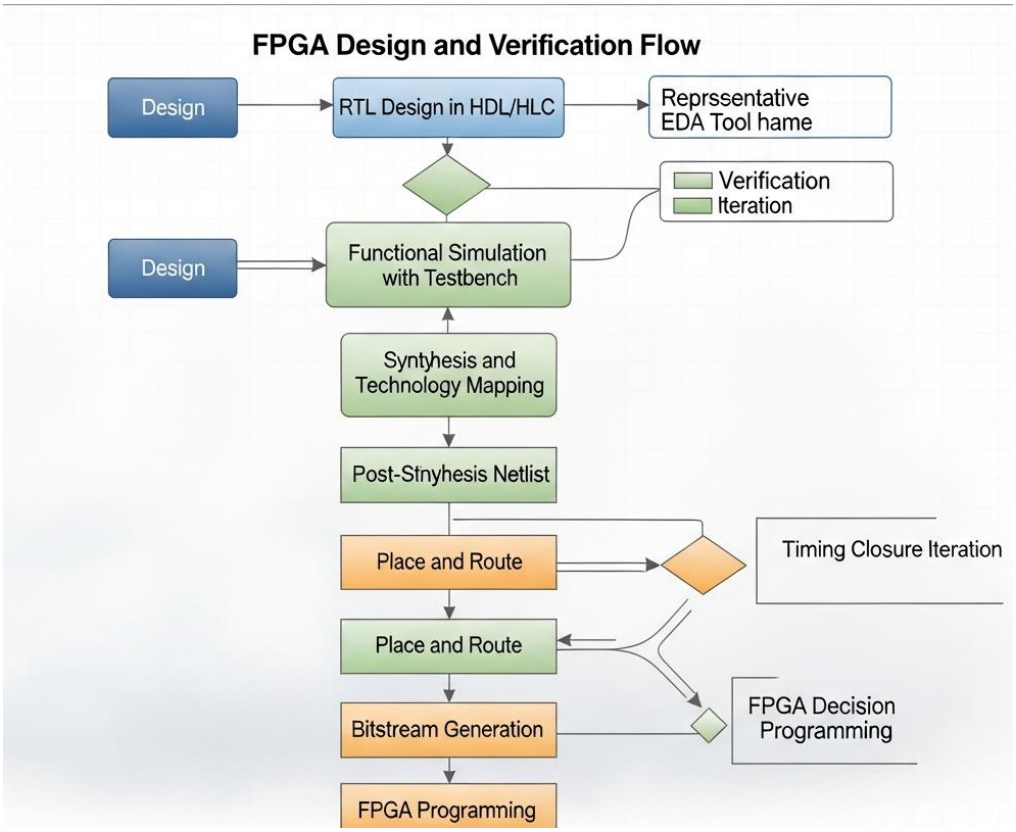

Figure 4.1: *Complete FPGA design and verification flow from RTL specification to bitstream generation, illustrating iterative timing closure and the integration of functional and timing verification stages.*

4.3 ASIC Design Flow and Fabrication

4.3.1 Full-Custom, Semi-Custom Design Flows, and Standard Cell Libraries

The ASIC design flow is a structured, multi-stage engineering process that transforms a behavioral specification into a verified, manufacturable physical layout. The flow is broadly categorized into front-end design, which encompasses specification, RTL coding, functional verification, and logic synthesis, and **back-end design** (also termed physical design or Place and Route), which covers

ISBN 978-816860178-9

floorplanning, placement, clock tree synthesis (CTS), routing, and physical verification. The boundary between these two phases is the gate-level netlist produced by logic synthesis, a technology-mapped description of the design in terms of the foundry's standard cell library. The complete flow for a complex SoC design at advanced nodes involves thousands of individual tool invocations, scripted design closure runs, and iterative signoff checks that collectively span several months of engineering effort (Lavagno et al., 2016).

Standard cell libraries are the fundamental building blocks of semi-custom ASIC design, comprising pre-characterized collections of logic gates, flip-flops, latches, multiplexers, and complex functions implemented as fixed-height, variable-width layout cells compatible with automated place-and-route tools. A production-quality standard cell library for a 28 nm process node may contain 600 to 1,200 distinct cell variants, including multiple drive strength options for each logic function (typically 1×, 2×, 4×, 8×, and 16× drive strength), low-voltage threshold (LVT), standard-voltage threshold (SVT), and high-voltage threshold (HVT) flavors for power-performance optimization, and specialized cells for scan insertion, level shifting, and clock gating. Each cell is characterized across a **process-voltage-temperature (PVT) corner matrix** spanning fast-fast, typical-typical, and slow-slow process corners at supply voltages ranging from 0.72 V to 1.32 V and temperatures from −40°C to 125°C, producing Liberty (.lib) timing models that capture cell delays, transition times, and power consumption as functions of input slew and output load (Weste & Harris, 2010).

The table below presents representative parameters for standard cell libraries at selected CMOS technology nodes, illustrating the scaling

trends in cell density, operating voltage, and timing characteristics across process generations.

Table 4.1: Standard Cell Library Parameters Across CMOS Technology Nodes

Technology Node	Cell Height (Track)	Minimum Supply Voltage	Typical INV D1 Delay (ps)
28 nm CMOS	9-track	0.72 V	18–22 ps
16 nm FinFET	7.5-track	0.60 V	12–15 ps
7 nm FinFET	6-track	0.50 V	8–11 ps
5 nm GAA	5-track	0.45 V	5–7 ps

Full-custom design, employed for performance-critical blocks such as SRAMs, analog-digital interfaces, and ultra-high-speed I/O circuits, involves manual transistor-level layout where every device dimension, implant region, and metal routing segment is individually optimized by the designer. Full-custom cells achieve transistor densities and performance levels unattainable with automated place-and-route, but require 10–20× more engineering effort per unit area compared to standard cell design. SRAM bit cells, designed in full-custom style, achieve densities of **0.021 μm² per bit** in TSMC's 5 nm N5 process, enabling 32 MB of on-chip cache within an area of approximately 17 mm²—a density that would be impossible with standard logic cell implementations. The semi-custom approach using hard and soft IP macros for memory, high-speed interfaces (PCIe, DDR, USB), and processor cores allows design teams to leverage validated pre-existing blocks while focusing custom engineering effort on differentiating logic (Lavagno et al., 2016).

ISBN 978-816860178-9

4.3.2 Fabrication Processes, Physical Verification, and Economic Considerations

The fabrication of an ASIC proceeds through a sequence of photolithographic patterning, deposition, and etching steps that collectively define the transistor structures and metal interconnect layers constituting the finished integrated circuit. A modern 7 nm FinFET process involves over **1,000 individual process steps** across approximately 80–100 photolithographic mask layers, spanning front-end-of-line (FEOL) transistor formation and back-end-of-line (BEOL) interconnect metallization. Extreme Ultraviolet (EUV) lithography, employing 13.5 nm wavelength light generated by tin plasma sources, has become essential at 7 nm and below to pattern the critical gate, fin, and lower metal layers with the required dimensional precision and overlay accuracy. TSMC's N5 process, representing the 5 nm generation, achieves a logic cell density of approximately **173 MTr/mm²** and has been adopted for high-volume production of Apple A14/A15 SoCs and AMD Ryzen 5000 series processors (TSMC, 2022).

Physical verification encompasses the rule-based and simulation-based checks applied to the completed layout to ensure compliance with the foundry's design rule manual (DRM) and to confirm electrical correctness. **Design Rule Checking (DRC)** verifies that all geometric dimensions, spacing, enclosure, and density rules specified by the foundry are satisfied, flagging violations that could cause lithographic printing failures or manufacturing defects. Layout Versus Schematic (LVS) verification extracts the transistor netlist from the physical layout and compares it against the schematic netlist to confirm topological equivalence, detecting missing connections, short circuits, and incorrect device sizing. Parasitic Extraction (PEX)

computes the resistance and capacitance of all layout conductors from their geometric properties, enabling post-layout simulation that accurately predicts the circuit's performance under realistic loading conditions—critical for high-speed interfaces where interconnect parasitics can degrade signal integrity by tens of picoseconds.

The economic calculus of ASIC versus FPGA implementation is governed primarily by production volume and the balance between NRE cost amortization and per-unit manufacturing cost savings. The NRE cost for a complete mask set in TSMC's 7 nm process is approximately **$30–50 million**, while a wafer costs approximately $10,000–15,000, yielding a die cost that decreases with increasing production volume as fixed NRE costs are amortized. At production volumes below approximately 50,000 units, FPGAs typically offer lower total cost of ownership despite their higher per-unit price ($20–500 per device) because the NRE investment is avoided entirely. Above this volume threshold, the ASIC's lower manufacturing cost ($1–20 per die at scale) and superior power efficiency—typically **5–10× lower power than an equivalent FPGA implementation**—justify the NRE investment and extended development timeline (Kuon & Rose, 2007).

Figure 4.2 presents the ASIC physical design flow from synthesized netlist through floorplanning, placement, clock tree synthesis, routing, and physical verification sign-off, indicating the iterative loops and tool categories employed at each stage.

ISBN 978-816860178-9

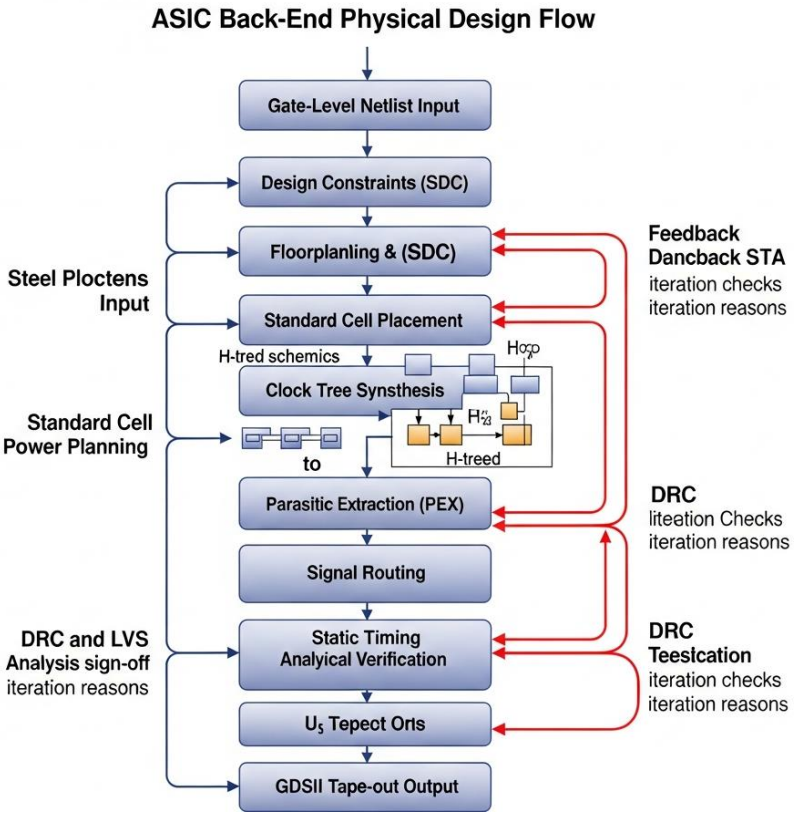

Figure 4.2: *ASIC back-end physical design flow from gate-level netlist to GDSII tape-out, illustrating iterative timing closure and physical verification sign-off stages including CTS, PEX, STA, DRC, and LVS.*

4.4 Verification and Testing Techniques

4.4.1 Functional Verification, Timing Analysis, and Fault Coverage

Verification is the process of confirming that a design correctly implements its specification across all intended operating conditions, and it represents the single largest consumer of engineering resources in modern ASIC and FPGA development. Industry surveys consistently indicate that verification consumes **50–70% of total design project effort**, and the probability that a first silicon ASIC requires re-spin due to functional bugs remains approximately 50–60% despite decades of advances in verification methodology (Wilson, 2020). The complexity of verification scales super-linearly with design

size, as the interaction space between functional blocks grows combinatorially with the number of state-holding elements and interface protocols. A billion-gate SoC design may contain over 10^8 flip-flops, making exhaustive simulation infeasible and necessitating a structured combination of simulation, formal verification, emulation, and hardware prototyping.

Simulation-based verification employs constrained-random test generation to explore the design's functional space efficiently. A SystemVerilog/UVM testbench generates randomized stimulus within user-defined constraints, applies it to the Design Under Verification (DUV), and checks responses against a golden reference model. **Functional coverage** monitors which design states, transitions, and input combinations have been exercised during simulation, providing a quantitative measure of verification completeness. Coverage-driven verification iterates between coverage analysis and test constraint refinement, focusing simulation effort on uncovered scenarios until all coverage points are satisfied. Formal property verification, using tools such as Cadence JasperGold and Synopsys VC Formal, mathematically proves or disproves assertions about the design's behavior using model checking and equivalence checking algorithms, providing exhaustive verification of specific properties—such as FIFO overflow prevention or protocol handshake correctness—that are difficult to cover reliably through simulation (Bergeron, 2006).

Static Timing Analysis (STA) is the industry-standard methodology for verifying that a design meets its timing constraints without performing dynamic simulation. STA tools traverse the timing graph of the placed-and-routed netlist, computing the worst-case signal

ISBN 978-816860178-9

arrival times and required times at every sequential element under all specified PVT corners. A setup timing violation occurs when a signal arrives at a flip-flop's data input less than the required setup time before the clock edge, potentially causing metastability and incorrect state capture. Hold violations, conversely, occur when a signal changes too rapidly after the clock edge, risking capture of the wrong data value. Modern STA tools perform on-chip variation (OCV) analysis using statistical static timing analysis (SSTA) to account for within-die process variations, applying timing derating factors of **5–15%** to account for random and systematic variations in transistor threshold voltage and interconnect dimensions across the die (Weste & Harris, 2010).

- **Equivalence checking** tools such as Synopsys Formality verify logical equivalence between RTL and post-synthesis gate-level netlists, and between pre- and post-layout netlists after engineering change orders (ECOs), replacing re-simulation with a complete formal proof of functional identity.
- **Power analysis** using switching activity annotation from simulation (SAIF files) enables accurate estimation of dynamic power consumption at the gate and block level, with modern SoC designs targeting **dynamic power densities below 0.3 W/mm²** to satisfy thermal and battery life constraints.
- The **IEEE 1149.1 JTAG boundary scan standard** mandates a serial scan chain connecting all I/O cells around the device perimeter, enabling structural testing of board-level interconnects with fault coverage exceeding 98% for stuck-at faults on PCB nets.

SRR Publicizing Research

4.4.2 Case Study: Silicon Debug and Test Implementation in Apple A-Series SoC

Background: Apple's A-series application processors represent the most commercially successful series of mobile ASIC designs, with cumulative production exceeding one billion units across iPhone, iPad, and iPod product lines. The Apple A15 Bionic, fabricated in TSMC's N5P (5 nm enhanced) process, integrates approximately **15 billion transistors** across a die area of 107.7 mm², incorporating a 6-core CPU, 4-core GPU, 16-core Neural Engine, image signal processor, secure enclave, and multiple dedicated hardware accelerators. The verification and test challenges posed by a design of this complexity are substantial: ensuring that every functional block operates correctly across the full operating range of 0.8 V to 1.25 V supply voltage and −20°C to 85°C junction temperature, and that manufacturing test can detect the full range of potential fabrication defects with sufficient yield-correlated fault coverage (Apple Inc., 2021).

Implementation Details: Apple's verification methodology for the A15 employed a multi-layered approach combining block-level UVM simulation environments, full-chip gate-level simulation with back-annotated parasitics, formal property verification for the CPU pipeline's memory ordering model and cache coherency protocol, and a 64-FPGA emulation platform for software bring-up and pre-silicon OS validation. The manufacturing test strategy employed **Automatic Test Pattern Generation (ATPG)** using Mentor Tessent and Synopsys TetraMAX tools, generating scan chain test patterns targeting stuck-at, transition, and path delay fault models across over 200 independent scan chains containing approximately 50 million

ISBN 978-816860178-9

flip-flops. Achieving 99.5% stuck-at fault coverage required approximately 8,000 test patterns, applied at an ATE (Automatic Test Equipment) data rate of 400 MHz, resulting in a total test time of approximately 2.4 seconds per device at production test—a critical parameter given the need to test hundreds of millions of devices annually.

Technologies Used: The test infrastructure embedded within the A15 SoC includes IEEE 1500 wrapper cells around each major functional core, enabling hierarchical test access and allowing individual cores to be tested independently before full-chip integration testing. Built-In Self-Test (BIST) circuits are implemented for all on-chip SRAM macros, using March algorithm-based memory BIST controllers that test each SRAM array for stuck-at, coupling, and retention faults without requiring external memory test patterns. On-chip voltage and temperature sensors, ring oscillator-based process monitors, and per-core performance counters provide parametric characterization data logged during production test, enabling statistical process control and facilitating early detection of process excursions that could affect reliability or performance binning of the final product.

Social Need and Impact: The rigorous verification and test methodology applied to high-volume mobile SoCs like the Apple A15 directly underpins the reliability and safety of devices that billions of people depend on for communication, navigation, health monitoring, and emergency services. A latent functional bug or undetected manufacturing defect in a safety-critical path could cause device failure in life-threatening situations—cardiac monitoring apps, emergency location services, or driver assistance features on CarPlay-enabled vehicles. The energy efficiency gains enabled by well-verified,

optimally implemented ASIC designs translate directly to **extended battery life**, with the A15's power efficiency enabling flagship smartphone performance at an average system power of under 4 W, reducing the energy consumption of over one billion active devices by tens of terawatt-hours annually compared to less efficient alternatives (Apple Inc., 2021).

4.5 Summary

FPGA and ASIC implementation techniques collectively represent the practical realization pathway for the digital algorithms and architectures developed at higher levels of abstraction in the VLSI design hierarchy. This section examined the programmable logic architectures and HDL-based design flows that make FPGAs the preferred platform for rapid prototyping and flexible deployment, alongside the structured ASIC design flow from RTL specification through standard cell synthesis, physical design, and tape-out that enables the performance, power, and density levels demanded by high-volume consumer and enterprise applications. The critical economic trade-offs between FPGA and ASIC approaches were quantified in terms of NRE investment, per-unit cost, and power efficiency. Comprehensive verification and testing methodologies, illustrated through the Apple A15 case study, demonstrated how simulation, formal methods, ATPG, and BIST collectively ensure functional correctness and manufacturing quality at billion-unit production scales.

References

[1] Apple Inc. (2021). *A15 Bionic: The world's fastest smartphone chip*. Apple Newsroom. https://www.apple.com/newsroom/2021/09/apple-unveils-a15-bionic

ISBN 978-816860178-9

[2] Bergeron, J. (2006). *Writing testbenches using SystemVerilog*. Springer.

[3] Coussy, P., & Morawiec, A. (2008). *High-level synthesis: From algorithm to digital circuit*. Springer.

[4] Grand View Research. (2023). *Field programmable gate array (FPGA) market size, share & trends analysis report*. Grand View Research.

[5] Intel Corporation. (2022). *Intel Agilex FPGA and SoC device overview*. Intel Technical Documentation. https://www.intel.com/content/www/us/en/products/details/fpga/agilex.html

[6] Kuon, I., & Rose, J. (2007). Measuring the gap between FPGAs and ASICs. *IEEE Transactions on Computer-Aided Design of Integrated Circuits and Systems, 26*(2), 203–215. https://doi.org/10.1109/TCAD.2006.884574

[7] Lavagno, L., Scheffer, L., & Martin, G. (2016). *Electronic design automation for integrated circuits handbook* (2nd ed.). CRC Press.

[8] Synopsys. (2022). *HAPS-100 FPGA-based prototyping system datasheet*. Synopsys Inc. https://www.synopsys.com/verification/prototyping/haps.html

[9] Trimberger, S. M. (2018). Three ages of FPGAs: A retrospective on the first thirty years of FPGA technology. *Proceedings of the IEEE, 106*(10), 1720–1735. https://doi.org/10.1109/JPROC.2018.2834746

[10] TSMC. (2022). *TSMC N5 process technology*. Taiwan Semiconductor Manufacturing Company. https://www.tsmc.com/english/dedicatedFoundry/technology/logic/l_5nm

[11] Weste, N. H. E., & Harris, D. M. (2010). *CMOS VLSI design: A circuits and systems perspective* (4th ed.). Addison-Wesley.

[12] Wilson, R. (2020). *2020 Wilson research group functional verification study*. Mentor, A Siemens Business.

SRR Publicizing Research

Section 5

AI-Driven VLSI and DSP Optimization

5.1 Introduction

The increasing complexity of modern **Very Large Scale Integration (VLSI)** systems and Digital Signal Processing (DSP) algorithms has rendered traditional manual and rule-based design methodologies fundamentally insufficient for meeting the performance, power, and time-to-market demands of contemporary semiconductor products. A leading-edge SoC design at the 3 nm process node may contain upward of 20 billion transistors, hundreds of distinct functional blocks, and thousands of timing and power constraints that must be simultaneously satisfied across dozens of process-voltage-temperature corners—a combinatorial optimization problem of a scale that exceeds the practical limits of human engineering intuition and deterministic algorithmic approaches. Artificial intelligence, and machine learning in particular, has emerged as the transformative methodology that enables design teams to navigate this complexity by learning from historical design data, predicting outcomes before expensive simulation, and autonomously optimizing design parameters across vast solution spaces (Kahng, 2018).

The shift toward **intelligent design automation** represents a fundamental paradigm change in the Electronic Design Automation (EDA) industry, moving from rule-based tools that encode expert knowledge in deterministic algorithms toward data-driven systems that extract optimization strategies directly from design corpora. This transition has been catalyzed by three converging factors: the exponential growth in available design data from successive product

ISBN 978-816860178-9

generations, the maturation of deep learning architectures capable of modeling complex nonlinear relationships between design parameters and outcomes, and the availability of GPU-accelerated computing infrastructure that makes training large models on design datasets computationally feasible. Major EDA vendors including Synopsys, Cadence, and Siemens EDA have embedded ML capabilities into their flagship tools, while AI-native EDA startups such as Cerebrus, Synopsys DSO.ai, and Cadence Cerebrus have demonstrated **10–25% power-performance-area (PPA) improvements** over expert-tuned baseline flows on production designs (Khailany et al., 2020).

In the domain of DSP, artificial intelligence has catalyzed a parallel revolution by enabling signal processing systems that adapt to their operational environment, learn optimal processing strategies from data, and execute complex recognition and inference tasks that are intractable with classical filter-based approaches. Neural network-based signal processing has displaced conventional algorithms in speech recognition, audio enhancement, channel equalization, radar target classification, and biomedical signal interpretation, achieving accuracy levels that approach or exceed human performance on many benchmark tasks. The integration of AI inference engines directly into DSP hardware—exemplified by the Neural Processing Units (NPUs) in mobile SoCs and the AI-optimized DSP cores in Qualcomm's Hexagon architecture—reflects the convergence of these two disciplines into a unified intelligent signal processing paradigm (LeCun et al., 2015).

The scope of AI applications in VLSI and DSP spans the entire design and deployment lifecycle, from early-stage design space exploration and architectural selection through physical implementation

optimization, manufacturing yield prediction, post-silicon validation, and real-time adaptive signal processing in deployed systems. This section provides a structured examination of machine learning applications in VLSI design, AI-driven DSP algorithm optimization, and intelligent design automation frameworks, supported by quantitative performance data, case studies from production implementations, and an analysis of the technical challenges and opportunities that define the frontier of this rapidly evolving field.

5.2 Machine Learning in VLSI Design

5.2.1 Design Space Exploration, Predictive Modeling, and EDA Integration

Design space exploration (DSE) is the process of evaluating a large number of candidate design configurations—differing in microarchitectural parameters, synthesis constraints, floorplan strategies, and implementation options—to identify configurations that optimally balance performance, power, area, and other design objectives. In conventional practice, DSE is performed by running complete synthesis and simulation flows on a representative sample of design points, a process that may require hours to days per evaluation and limits the explorable design space to a few hundred configurations at best. **Machine learning surrogate models** trained on a modest initial dataset of fully evaluated design points can predict PPA outcomes for unevaluated configurations in milliseconds, enabling the exploration of design spaces containing millions of points with a total computational cost comparable to evaluating a few hundred points through full simulation (Reagen et al., 2017).

Regression models including Gaussian Process Regression (GPR), Random Forest, Gradient Boosting (XGBoost), and deep neural

ISBN 978-816860178-9

networks have all been applied to PPA prediction with reported mean absolute errors of **3–8% for timing** and **5–12% for power** estimates relative to fully implemented designs, compared to errors of 20–40% typical of early-stage analytical models. GPR is particularly well-suited to DSE applications because it provides not only a point prediction but also a confidence interval, enabling active learning strategies that direct exploration toward regions of high uncertainty or predicted optimality. Bayesian optimization frameworks that combine GPR surrogate models with acquisition functions such as Expected Improvement (EI) or Upper Confidence Bound (UCB) have been demonstrated to find near-optimal microarchitectural configurations for processor cache hierarchies and memory subsystems in 10–50 evaluations, compared to hundreds or thousands required by grid search or random sampling (Nardi et al., 2019).

The integration of ML models directly into EDA tool flows has progressed substantially, with Synopsys DSO.ai representing the most publicly documented commercial implementation. DSO.ai employs a reinforcement learning agent that autonomously sets synthesis and implementation tool directives—including synthesis effort levels, optimization strategies, clock gating aggressiveness, and placement constraints—and receives PPA outcomes as reward signals after each complete implementation run. Over successive iterations, the RL agent learns a policy that maps design state representations to tool directive configurations, converging toward a near-optimal implementation strategy for the specific design. Published results from production deployments at Intel, Samsung, and Renesas report **PPA improvements of 10–25%** over expert-tuned baseline flows, achieved with reduced human engineering time (Synopsys, 2022).

SRR Publicizing Research

- **Graph Neural Networks (GNNs)** operating on netlist representations model the design as a graph of logic cells and interconnects, enabling prediction of post-route congestion and timing violations directly from the synthesized netlist with accuracy sufficient to guide early placement decisions before full routing.
- **Transfer learning** techniques allow ML models trained on historical designs from previous product generations to be fine-tuned on small datasets from new designs, reducing the data requirements for accurate PPA prediction by **60–80%** and making ML-based DSE practical even for design teams with limited historical data.
- Reinforcement learning agents trained for **clock tree synthesis** optimization have demonstrated the ability to autonomously balance clock skew, insertion delay, and power consumption, achieving clock tree implementations with 15% lower power than those produced by conventional CTS tools on benchmark designs.

5.2.2 Fault Detection, Yield Prediction, and Manufacturing Intelligence

Semiconductor manufacturing yield—the fraction of fabricated die that pass all functional and parametric tests—is the primary determinant of wafer fabrication economics and directly governs the cost structure of ASIC production. Yield loss arises from two distinct mechanisms: systematic yield loss attributable to design-process interactions such as lithographic hotspots, chemical-mechanical planarization (CMP) density violations, and electromigration-prone routing topologies; and random defect yield loss caused by particulate

ISBN 978-816860178-9

contamination, oxide pinholes, and other stochastic manufacturing imperfections. **Machine learning models** trained on historical yield data, process metrology measurements, and design layout features have demonstrated remarkable capability in predicting end-of-line yield from early-stage in-line measurements, enabling proactive identification and correction of yield-limiting conditions before a complete wafer lot is processed (Cunningham, 2019).

Convolutional neural networks (CNNs) applied to wafer-level defect map images have achieved defect classification accuracies exceeding **98.5%** across defect categories including scratch patterns, edge die failures, ring-shaped clustering, and center-type defect distributions—performance that matches or exceeds expert human classification while operating at throughputs of thousands of wafer maps per minute. These models, trained on millions of historical wafer maps from foundry databases, learn to recognize subtle spatial signatures associated with specific process equipment malfunctions or chemical imbalances, enabling rapid root cause identification and equipment preventive maintenance scheduling. Foundries including TSMC and Samsung Foundry have integrated CNN-based defect classification into their automated process control (APC) systems, reporting yield improvements of **2–5 percentage points** on mature process nodes through faster defect response cycles (Chen et al., 2020).

Figure 5.1 illustrates the ML-driven yield prediction pipeline, depicting the flow from in-line process measurement data and layout feature extraction through machine learning model training, yield prediction, and feedback to design and process optimization loops.

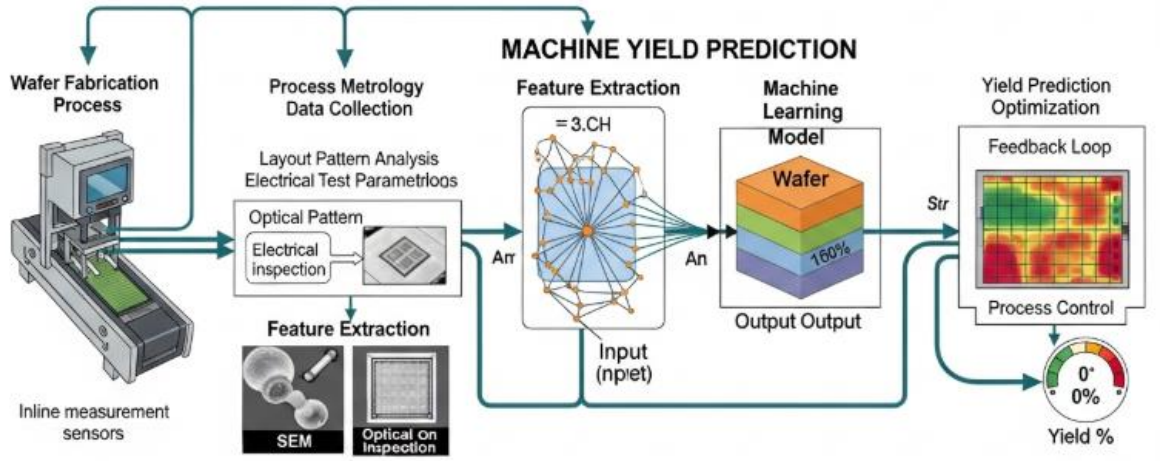

Figure 5.1: *Machine learning yield prediction pipeline integrating in-line process metrology, layout feature extraction, neural network inference, and feedback to design and process optimization control loops.*

Lithographic hotspot detection using ML represents another high-impact application where deep learning has substantially improved upon rule-based approaches. Traditional Design Rule Checking (DRC) and optical proximity correction (OPC) verification tools identify potential lithographic failures using geometric rules calibrated to the process design kit, but struggle to capture complex multi-feature interactions that cause printing failures in dense layouts. CNN models trained on lithographic simulation results learn to recognize hotspot-inducing layout patterns with a **false negative rate below 0.1%** and a false positive rate of 5–10%, compared to false negative rates of 2–5% for rule-based tools—a critical improvement given that a single undetected lithographic hotspot in a high-volume design can cause millions of defective die. These models operate at speeds 100–1000× faster than full lithographic simulation, enabling their integration into interactive layout editors for real-time hotspot feedback during physical design (Jiang et al., 2019).

ISBN 978-816860178-9

5.3 AI in DSP Algorithm Optimization

5.3.1 Adaptive Filtering, Neural Signal Processing, and Pattern Recognition

Classical adaptive filtering algorithms such as the Least Mean Squares (LMS) and Recursive Least Squares (RLS) adjust filter coefficients iteratively to minimize a defined error criterion, enabling signal processing systems to track slowly varying channel characteristics in applications including acoustic echo cancellation, channel equalization, and noise suppression. While these algorithms are mathematically elegant and computationally efficient, their performance degrades significantly in environments with **non-stationary statistics**, nonlinear distortions, or multipath interference structures that violate the linear filtering assumption. AI-based adaptive filtering approaches, employing recurrent neural networks, Long Short-Term Memory (LSTM) architectures, and attention mechanisms, overcome these limitations by learning nonlinear input-output mappings from training data, achieving noise reduction performance 8–15 dB superior to LMS-based methods in challenging acoustic environments (Sayed, 2008).

Deep learning has fundamentally transformed speech and audio signal processing, replacing elaborate hand-engineered feature extraction pipelines with end-to-end learned representations that capture both spectral and temporal signal structure at multiple scales. **Convolutional neural networks** applied to Short-Time Fourier Transform (STFT) magnitude spectrograms learn hierarchical feature detectors—from low-level spectral patterns at shallow layers to phonetic and prosodic representations at deeper layers—enabling speech recognition word error rates below 3% on standard

benchmarks, compared to 10–15% for the best classical Hidden Markov Model (HMM) systems. In wireless communications, deep neural network-based channel estimators trained on statistical channel models achieve mean squared error (MSE) performance **2–4 dB below** LMMSE estimators in doubly-selective fading channels, by exploiting learned knowledge of channel correlation structure that is unavailable to model-based estimators operating without exact channel statistics (O'Shea & Hoydis, 2017).

Pattern recognition in signals—the identification of specific signal structures, events, or classes within a continuous data stream—represents one of the earliest and most successful application domains for neural network-based DSP. Electrocardiogram (ECG) arrhythmia detection using deep convolutional networks trained on annotated Holter monitor recordings has achieved sensitivity and specificity exceeding **99% for atrial fibrillation** detection on held-out test sets, matching board-certified cardiologist performance on the same datasets. Radar automatic target recognition (ATR) using micro-Doppler signature analysis with convolutional LSTM networks distinguishes between pedestrians, cyclists, vehicles, and drones with classification accuracies exceeding 97% at signal-to-noise ratios above 10 dB, enabling reliable operation in cluttered urban environments where classical Doppler processing fails due to overlapping radar cross-section signatures (Kim & Moon, 2016).

- **Transformer architectures** with self-attention mechanisms applied to raw I/Q sample sequences in software-defined radio receivers achieve modulation classification accuracies of **98.3%** across 24 modulation types at SNR above 6 dB, enabling cognitive radio systems that autonomously identify and adapt

ISBN 978-816860178-9

to the radio frequency environment without prior knowledge of signal parameters.

- Deep reinforcement learning applied to **adaptive beamforming** in phased array antenna systems learns optimal weight vectors for interference nulling and target tracking in real time, achieving interference rejection exceeding 40 dB in scenarios with multiple rapidly moving interference sources where classical adaptive beamforming algorithms diverge.
- Spiking Neural Networks (SNNs) implemented on neuromorphic processors such as Intel Loihi achieve **ultra-low-power** keyword spotting at 100–500 μW—10–50× lower power than equivalent CNN implementations—by exploiting sparse temporal coding and event-driven processing to eliminate computation during silent intervals.

5.3.2 Real-Time AI Optimization and Hardware Acceleration

The deployment of AI-based DSP algorithms in real-time embedded systems demands hardware implementations capable of executing neural network inference within stringent latency and power budgets while processing continuous input streams. A 5G NR baseband receiver incorporating a deep learning channel estimator must complete inference within the **OFDM symbol duration of 71.4 μs** (for 15 kHz subcarrier spacing) to avoid buffering latency that would violate the strict timing requirements of the physical layer uplink processing chain. Meeting this constraint with a network containing millions of parameters requires dedicated neural network accelerator hardware implementing dense matrix-vector multiplication in highly parallel systolic array or vector processing architectures, achieving

throughputs measured in TOPS (Tera-Operations Per Second) within power envelopes of a few watts (Sze et al., 2017).

Figure 5.2 illustrates the hardware architecture of a dedicated neural network inference accelerator for real-time DSP applications, depicting the systolic array data path, on-chip weight buffer hierarchy, activation quantization pipeline, and interface to the DSP front-end signal acquisition subsystem.

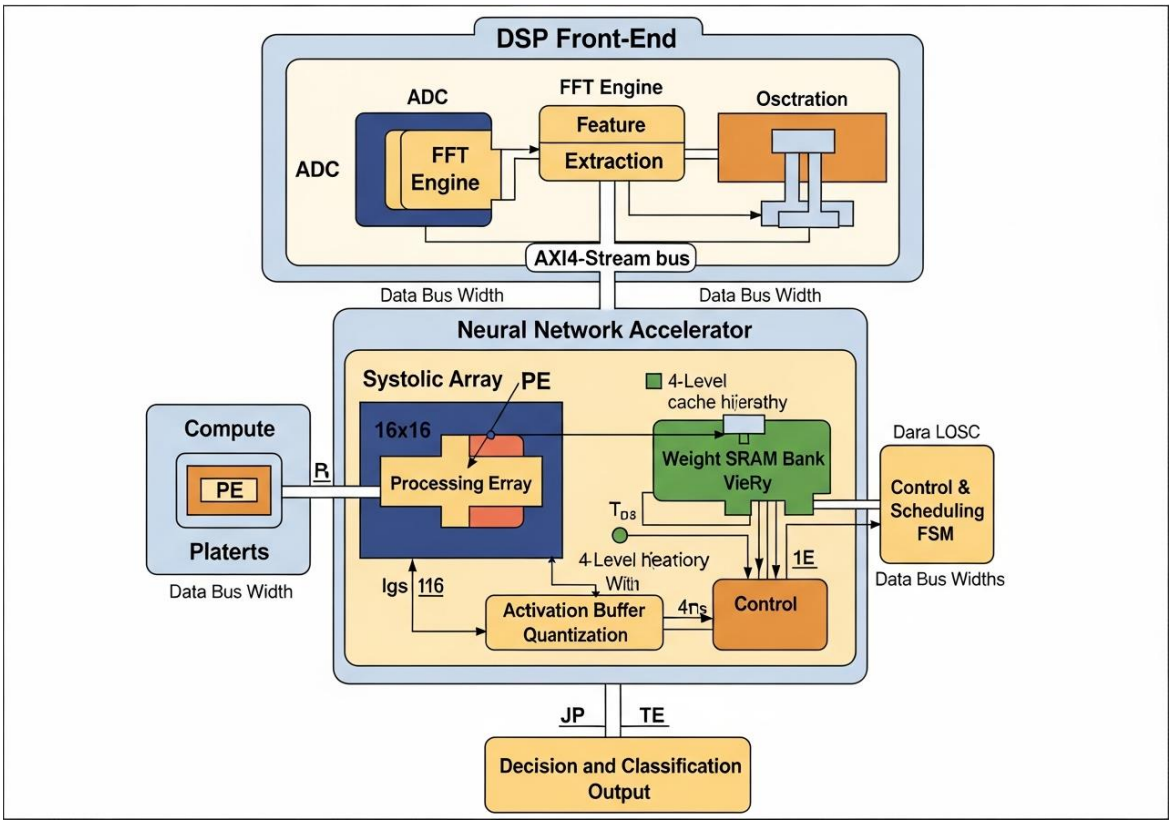

Figure 5.2: *Hardware architecture of a real-time neural network inference accelerator for DSP applications, illustrating the systolic array data path, weight buffer hierarchy, quantization pipeline, and DSP front-end integration.*

Neural network quantization is the primary technique for reducing the computational and memory cost of AI inference in DSP hardware, replacing 32-bit floating-point weights and activations with 8-bit, 4-bit, or even binary fixed-point representations. Post-training

ISBN 978-816860178-9

quantization of a MobileNetV3 image classification network from FP32 to INT8 reduces model size by **4×** and inference latency by 2–3× on ARM NEON SIMD hardware with less than 1% accuracy degradation, while quantization-aware training with 4-bit activations can recover most of the accuracy loss at an additional 2× computational reduction. For DSP-specific networks such as convolutional beamformers and adaptive equalizers, network pruning techniques that remove weight connections below a magnitude threshold achieve 80–95% sparsity with less than 0.5 dB SNR degradation, enabling sparse matrix acceleration hardware to deliver **5–10× energy efficiency improvements** over dense inference engines (Han et al., 2016).

5.4 Intelligent Design Automation Techniques

5.4.1 AI-Driven Placement, Routing, and Power-Timing Optimization

Physical design automation—the process of determining the physical locations of logic cells and the routing paths of signal nets within an integrated circuit layout—is among the most computationally intensive optimization problems in engineering, involving billions of variables, nonlinear objective functions, and complex interdependencies between placement quality, routing congestion, and timing performance. Traditional place-and-route tools employ deterministic algorithms including simulated annealing for placement, negotiation-based routing for global and detailed routing, and gradient-based optimization for timing-driven refinement, achieving high-quality results but requiring extensive expert-configured constraint files and tool directive tuning. **Deep reinforcement learning** applied to chip floorplanning, as

demonstrated by the landmark Nature paper from Google Brain (Mirhoseini et al., 2021), trained an RL agent on 10,000 chip netlists to place macro blocks and standard cell clusters, producing floorplans in under six hours that matched or exceeded human expert quality on all PPA metrics—a result that generated significant industry attention and controversy regarding the generalizability of the approach.

Table 5.1: Applications of AI and Machine Learning in VLSI and DSP Design Automation

Section	Key Focus Area	Techniques / Methods	Design Impact
ML in VLSI Design	Design Space Exploration	Supervised/unsupervised learning models	Faster and optimized design choices
ML in VLSI Design	Performance & Yield Prediction	Regression models, classification, fault detection	Improved reliability and manufacturing yield
AI in DSP Optimization	Adaptive & Neural Signal Processing	Adaptive filtering, neural networks	Enhanced signal accuracy and adaptability
AI in DSP Optimization	Pattern Recognition & Real-Time Tuning	AI-based pattern detection, online optimization	Efficient real-time signal processing
Intelligent Design Automation	AI-Driven Physical & Logical Design	Placement/routing algorithms, metaheuristics	Reduced power, delay, and improved timing

Cadence Cerebrus, the commercial RL-based implementation optimization platform, employs a multi-agent reinforcement learning framework where individual agents specialize in different aspects of the physical design flow—placement legalization, clock tree topology selection, routing layer assignment, and power grid sizing—and coordinate through a shared reward signal derived from final PPA outcomes. Production deployments at leading fabless semiconductor

ISBN 978-816860178-9

companies have reported **QoR (Quality of Results) improvements of 10–20% in timing closure** and 8–15% in leakage power reduction compared to expert-tuned conventional flows, with the additional benefit of dramatically reduced manual constraint tuning time. The RL agent's learned policy encodes design-specific optimization strategies that generalize across implementation runs of the same design, enabling consistent high-quality results even when design parameters change between tape-out runs (Cadence Design Systems, 2022).

Power optimization in digital VLSI designs increasingly leverages ML models to predict the switching activity of internal nodes—the primary driver of dynamic power consumption—from simulation traces, enabling accurate power estimation without the prohibitive runtime of full gate-level simulation with back-annotated parasitics. Recurrent neural networks trained on short simulation windows predict the time-averaged switching activity of un-simulated nodes with **mean absolute error below 4%**, enabling full-chip dynamic power estimation at speeds 50–100× faster than exhaustive gate-level simulation. This capability is deployed in power-aware synthesis flows that use predicted switching activity to guide clock gating insertion, operand isolation logic optimization, and multi-threshold cell assignment, collectively achieving dynamic power reductions of 20–30% with less than 2% timing degradation compared to power-unaware baseline flows (Dong et al., 2019).

5.4.2 Case Study: Google's AI-Driven Chip Design for TPU

Background: Google's Tensor Processing Units (TPUs) are custom ASICs designed specifically to accelerate the matrix multiplication operations that dominate deep learning training and inference

workloads. The TPU design problem presents a particularly well-suited application for AI-driven design automation: each successive TPU generation must integrate increasingly large systolic arrays, high-bandwidth memory interfaces, and complex on-chip networks while meeting aggressive power density targets dictated by Google's data center thermal management infrastructure. The floorplanning of a TPU chip—determining the physical placement of large functional blocks including the matrix multiply units, activation memory, unified buffer, and interconnect fabric—has a profound impact on wire length, routing congestion, and ultimately the chip's clock frequency and power consumption (Jouppi et al., 2017).

Implementation Details: Google Brain's chip placement research team applied a deep reinforcement learning approach to automate TPU floorplanning, training a graph neural network policy using a dataset of 10,000 previously designed chip blocks with their associated placement outcomes and PPA metrics. The policy network receives a graph representation of the chip netlist—encoding connectivity, cell sizes, and timing criticality—and sequentially places each macro and standard cell cluster onto a discrete placement grid, receiving reward signals based on post-placement wirelength, congestion, and timing estimates. After training, the policy generates a complete **floorplan for a new TPU block within 6 hours**, compared to the 2–3 weeks required by human expert engineers for a comparable manual floorplanning effort. The AI-generated floorplans matched human expert quality on wirelength and congestion metrics and achieved **superior timing results** on 3 of 5 evaluated TPU block designs (Mirhoseini et al., 2021).

ISBN 978-816860178-9

Technologies Used: The placement policy is implemented as a 3-layer Graph Convolutional Network (GCN) processing the chip netlist graph, followed by a 3-layer fully connected network that outputs placement actions. Training employs the Proximal Policy Optimization (PPO) reinforcement learning algorithm with a curriculum strategy that progressively increases placement problem difficulty, starting with small netlists of 50 macros and scaling to full TPU blocks with over 750 macros and tens of thousands of standard cell clusters. The reward function combines normalized wirelength, routing congestion estimated by a fast analytical model, and timing criticality violations, with weights tuned to reflect the relative importance of each metric in the final PPA outcome. Infrastructure-wise, training runs on 512 Google TPU v3 cores for approximately 12 hours per training campaign, demonstrating a productive recursion where TPU hardware accelerates the RL training that optimizes TPU layout.

Social Need and Impact: The ability to automate and accelerate chip design using AI directly addresses one of the most significant bottlenecks in the semiconductor industry: the growing gap between chip design complexity and the availability of expert engineering talent. A typical advanced node SoC design requires a team of 500–1,000 engineers working for 2–4 years, at a total engineering cost that can exceed **$500 million** for the most complex designs. AI-driven design automation tools that reduce floorplanning effort from weeks to hours, or improve PPA by 15–20% without additional human effort, translate directly into faster product development cycles, lower design costs, and more efficient utilization of the scarce expert engineering workforce. These efficiency gains are critical for enabling the continued scaling of semiconductor capability that underpins

advances in healthcare diagnostics, climate modeling, autonomous transportation, and scientific computing that benefit society broadly (Kahng, 2018).

5.5 Summary

AI-driven VLSI and DSP optimization represents the most significant methodological shift in semiconductor design since the introduction of logic synthesis and automated place-and-route in the 1980s. This section examined how machine learning techniques—including deep neural networks, reinforcement learning, graph neural networks, and Bayesian optimization—are transforming design space exploration, yield prediction, lithographic hotspot detection, and physical implementation optimization in VLSI design flows. In DSP, the displacement of classical algorithms by deep learning-based approaches in adaptive filtering, channel estimation, speech recognition, and radar signal processing was quantified and contextualized within the hardware acceleration architectures that make real-time neural inference feasible. Intelligent design automation frameworks, culminating in the Google TPU AI floorplanning case study, demonstrated that autonomous design agents operating at the physical implementation level can match and in some dimensions exceed human expert engineering quality while compressing design timelines from weeks to hours. The convergence of AI methodology with semiconductor design practice is accelerating across all phases of the design lifecycle and is poised to become the dominant paradigm for navigating the complexity of future technology nodes.

ISBN 978-816860178-9

References

[1] Cadence Design Systems. (2022). *Cadence Cerebrus intelligent chip explorer: AI-driven RTL-to-GDS optimization*. Cadence White Paper. https://www.cadence.com/en_US/home/tools/digital-design-and-signoff/cerebrus.html

[2] Chen, Y., Huang, C., & Lin, Y. (2020). Machine learning applications in semiconductor manufacturing. *IEEE Transactions on Semiconductor Manufacturing, 33*(3), 412–425. https://doi.org/10.1109/TSM.2020.2995145

[3] Cunningham, S. (2019). The use of machine learning for yield improvement in semiconductor manufacturing. *Journal of Process Control, 71*, 1–12.

[4] Dong, Z., Chen, W., & Shi, W. (2019). Machine learning based dynamic power estimation for digital circuits. *Proceedings of the 56th ACM/IEEE Design Automation Conference (DAC)*, 1–6. https://doi.org/10.1145/3316781.3317847

[5] Han, S., Pool, J., Tran, J., & Dally, W. J. (2016). Learning both weights and connections for efficient neural networks. *Advances in Neural Information Processing Systems, 28*, 1135–1143.

[6] Jiang, Y., Yang, F., & Zeng, X. (2019). Efficient layout hotspot detection via binarized convolutional neural networks. *ACM Transactions on Design Automation of Electronic Systems, 24*(5), 1–22. https://doi.org/10.1145/3341684

[7] Jouppi, N. P., Young, C., Patil, N., & Patterson, D. (2017). In-datacenter performance analysis of a tensor processing unit. *Proceedings of the 44th International Symposium on Computer Architecture (ISCA)*, 1–12. https://doi.org/10.1145/3079856.3080246

[8] Kahng, A. B. (2018). New directions for learning-based IC design tools and methodologies. *Proceedings of the 23rd Asia and South Pacific Design Automation Conference (ASP-DAC)*, 405–410. https://doi.org/10.1109/ASPDAC.2018.8297362

[9] Khailany, B., Ren, H., Dai, S., & Godil, S. (2020). Accelerating chip design with machine learning. *IEEE Micro, 40*(6), 23–32. https://doi.org/10.1109/MM.2020.3026494

[10] Kim, Y., & Moon, T. (2016). Human activity classification based on micro-Doppler signatures using deep convolutional neural networks.

IEEE Transactions on Geoscience and Remote Sensing, 54(12), 7207–7216.

[11] LeCun, Y., Bengio, Y., & Hinton, G. (2015). Deep learning. *Nature, 521*(7553), 436–444. https://doi.org/10.1038/nature14539

[12] Mirhoseini, A., Goldie, A., Yazgan, M., & Dean, J. (2021). A graph placement methodology for fast chip design. *Nature, 594*(7862), 207–212. https://doi.org/10.1038/s41586-021-03544-w

[13] Nardi, L., Souza, B., & Koeplinger, D. (2019). Practical design space exploration. *Proceedings of the IEEE International Workshop on Rapid System Prototyping (RSP)*, 1–8.

[14] O'Shea, T., & Hoydis, J. (2017). An introduction to deep learning for the physical layer. *IEEE Transactions on Cognitive Communications and Networking, 3*(4), 563–575. https://doi.org/10.1109/TCCN.2017.2758370

[15] Reagen, B., Whatmough, P., & Adolf, R. (2017). Minerva: Enabling low-power, highly accurate deep neural network accelerators. *Proceedings of the 44th International Symposium on Computer Architecture*, 267–278.

[16] Synopsys. (2022). *DSO.ai autonomous design space optimization.* Synopsys Technical Brief. https://www.synopsys.com/implementation-and-signoff/signoff/dso-ai.html

ISBN 978-816860178-9

Section 6

Emerging Trends in Nanoelectronics and DSP Systems

6.1 Introduction

The semiconductor industry stands at a pivotal inflection point where the classical scaling paradigm embodied by Moore's Law—the empirical observation that transistor density doubles approximately every two years—is encountering fundamental physical, economic, and thermodynamic limits that necessitate a comprehensive rethinking of how computational systems are designed, fabricated, and operated. For five decades, performance improvements in electronic systems derived reliably from dimensional scaling of CMOS transistors, with each successive process node delivering smaller, faster, and more energy-efficient devices through geometric miniaturization of gate lengths, oxide thicknesses, and junction depths. However, as gate lengths have reached below **3 nm** in production silicon, quantum mechanical effects including direct source-to-drain tunneling, gate oxide leakage, and discrete dopant fluctuations have fundamentally altered transistor behavior, making classical long-channel device physics an inadequate basis for circuit design at these dimensions (Lundstrom & Jeong, 2013).

The imperative for innovation in **nano-scale electronic systems** extends beyond mere dimensional scaling to encompass fundamentally new device structures, novel materials, alternative computational substrates, and heterogeneous integration architectures that combine diverse technologies within a single package or system. Gate-All-Around (GAA) nanosheet transistors, which enclose the channel from all four sides with gate dielectric

material, have entered production at Samsung's 3 nm process node and provide superior electrostatic channel control compared to FinFET structures, reducing short-channel effects and enabling continued threshold voltage scaling. Beyond conventional silicon CMOS, research into two-dimensional materials including graphene and molybdenum disulfide (MoS_2), carbon nanotube field-effect transistors, and spin-based devices offers pathways to computational substrates with switching energies and device densities unachievable with silicon technology (Ferain et al., 2011).

The impact of these nanoelectronic advances on Digital Signal Processing systems is profound and multidimensional. Higher transistor densities enable more capable on-chip DSP engines with larger filter banks, deeper neural network inference pipelines, and more sophisticated signal conditioning chains within the same silicon footprint. New device characteristics—including the ambipolar transport behavior of carbon nanotube transistors and the non-volatile switching of memristors—introduce novel computational primitives that map naturally onto certain signal processing operations, offering pathways to in-memory computation architectures that eliminate the energy and bandwidth penalties of the conventional processor-memory interface. The convergence of nanoelectronics research with DSP systems design is therefore not an academic abstraction but a practical engineering frontier with direct implications for the capabilities of communication systems, medical devices, autonomous sensors, and high-performance computing platforms of the coming decade (Ionescu & Riel, 2011).

The scope of this section encompasses the most significant emerging device technologies and their scaling implications, the evolution of

ISBN 978-816860178-9

high-performance DSP systems toward AI integration and next-generation communication standards, and the forward-looking research directions in neuromorphic computing, 6G signal processing, heterogeneous integration, and sustainable electronics that will define the semiconductor landscape through 2040 and beyond. Together, these threads constitute the frontier at which materials science, device physics, circuit design, signal processing theory, and systems engineering converge to produce the next generation of electronic capability.

6.2 Nanoelectronics and Advanced Devices

6.2.1 FinFET, Gate-All-Around, and Beyond-CMOS Technologies

The FinFET (Fin Field-Effect Transistor) architecture, introduced into high-volume production at Intel's 22 nm node in 2012, represented the first fundamental departure from the planar MOSFET structure that had defined CMOS technology for four decades. In a FinFET, the channel region is formed as a thin vertical silicon fin rising above the substrate surface, with the gate electrode wrapping around three sides of the fin—top and both sidewalls—providing dramatically superior electrostatic control over channel potential compared to a single-gate planar device. This tri-gate structure reduces the subthreshold swing toward the theoretical thermionic limit of 60 mV/decade at room temperature, suppresses drain-induced barrier lowering (DIBL) to below **30 mV/V**, and enables continued threshold voltage scaling without the prohibitive increase in leakage current that limited planar CMOS scaling below 28 nm (Ferain et al., 2011).

Gate-All-Around (GAA) nanosheet transistors, commercialized by Samsung in their 3GAE process node in 2022, extend the FinFET concept to its logical conclusion by replacing the vertical fin with

horizontal stacked nanosheet channels—typically two to four silicon or silicon-germanium sheets with thicknesses of 5–8 nm—fully surrounded by high-k metal gate dielectric on all four sides. This geometry provides maximum electrostatic channel control, enabling gate lengths of 12–15 nm with subthreshold slopes within 5% of the ideal 60 mV/decade limit and effective oxide thicknesses (EOT) below **0.6 nm** achieved through hafnium zirconium oxide (HfZrO) high-k dielectrics deposited by atomic layer deposition. The nanosheet width is a configurable design parameter, allowing circuit designers to trade drive current against leakage by adjusting the total channel width through the number and width of nanosheets, a degree of freedom unavailable with fixed-fin-pitch FinFET technology. TSMC's equivalent architecture, termed N2 with Nanosheet FET, is scheduled for production in 2025 and is projected to deliver a **10–15% performance improvement** at iso-power compared to N3 FinFET (TSMC, 2023).

Beyond silicon-based CMOS scaling, a diverse portfolio of beyond-CMOS device technologies is being actively researched as potential complements or successors to transistor-based computation. Two-dimensional materials, particularly monolayer MoS_2 and WSe_2 transition metal dichalcogenides (TMDs), offer atomically thin semiconducting channels with intrinsic body thickness of 0.65 nm—far thinner than the thinnest achievable silicon nanosheets—enabling gate lengths below 1 nm with acceptable electrostatic control. Stanford researchers demonstrated an MoS_2 transistor with a physical gate length of **0.34 nm** using a single-walled carbon nanotube as the gate electrode, establishing a proof-of-concept for sub-nanometer transistors operating through quantum tunneling modulation rather than classical barrier control (Desai et al., 2016).

ISBN 978-816860178-9

Carbon nanotube field-effect transistors (CNFETs), exploiting the ballistic transport properties of semiconducting single-walled carbon nanotubes, have achieved switching energies below 1 aJ per operation at sub-1 V supply—approximately 5× lower than equivalent silicon CMOS—though achieving the nanotube purity and alignment precision required for large-scale integration remains a significant manufacturing challenge.

- **Negative Capacitance FETs (NC-FETs)** using ferroelectric hafnium oxide (HfO_2) gate dielectrics exploit ferroelectric polarization switching to amplify the gate voltage internally, achieving sub-60 mV/decade subthreshold slopes of **38 mV/decade** at room temperature and enabling logic operation at supply voltages below 0.3 V with conventional CMOS drive currents.
- **Tunnel FETs (TFETs)** operate via band-to-band quantum mechanical tunneling rather than thermionic injection, fundamentally decoupling subthreshold slope from the kT/q thermal limit and enabling ultralow-power switching at supply voltages below 0.5 V, making them attractive for IoT and biomedical sensor nodes where energy harvesting constrains available power to microwatts.
- **Spintronics devices**, including magnetic tunnel junctions (MTJs) and spin-orbit torque (SOT) switching elements, offer non-volatile logic and memory integration where computation state is encoded in the magnetic orientation of ferromagnetic layers rather than charge accumulation, potentially eliminating standby leakage power entirely in logic circuits.

6.2.2 Quantum Electronics, Molecular Devices, and Scaling Solutions

Quantum computing hardware represents the most radical departure from conventional binary CMOS logic, employing quantum mechanical superposition and entanglement to process information in fundamentally different ways that offer exponential computational advantages for specific problem classes including integer factorization, quantum chemistry simulation, and optimization. Current state-of-the-art quantum processors from IBM, Google, and IonQ employ superconducting qubit circuits operating at temperatures below **15 millikelvin**—achieved through dilution refrigerators consuming several kilowatts of cooling power—with qubit coherence times ranging from 100 μs for transmon qubits to 10 ms for fluxonium designs. Google's Sycamore processor, comprising 53 superconducting qubits, demonstrated quantum supremacy in 2019 by executing a specific sampling task in 200 seconds that classical supercomputers would require approximately 10,000 years to complete, though the practical relevance of this benchmark to real-world computation remains debated (Arute et al., 2019).

Molecular electronics—the use of individual molecules or small molecular assemblies as functional electronic components—represents the ultimate limit of device miniaturization, with molecular junctions occupying volumes of approximately 1 nm^3 compared to 50,000 nm^3 for a 5 nm FinFET. Experimentally demonstrated molecular devices include single-molecule diodes exhibiting rectification ratios exceeding $\mathbf{10^5}$, molecular transistors where the conductance of a single molecule is gated by a third electrode through electrostatic or electrochemical means, and

ISBN 978-816860178-9

molecular switches exploiting photoisomerization or conformational changes to toggle between high- and low-conductance states. The primary challenges impeding practical molecular electronics—reproducible molecular self-assembly over large areas, stable electrical contacts to individual molecules, and reliability under thermal fluctuations—remain active research topics, but recent advances in scanning tunneling microscope-based lithography and DNA-directed self-assembly have demonstrated pathways toward deterministic placement of molecular components with single-nanometer precision (Ratner, 2013).

Advanced packaging and heterogeneous integration have emerged as the practical near-term solution to the slowing of transistor-level scaling, enabling continued system-level performance scaling by combining multiple specialized chiplets—each fabricated at the optimal process node for its function—within a single package using advanced interconnect technologies. **3D chip stacking** using through-silicon vias (TSVs) and hybrid bonding achieves vertical interconnect pitches of 1–9 μm, enabling memory bandwidth densities exceeding 1 TB/s between stacked DRAM and logic dies as demonstrated in AMD's HBM-integrated Instinct MI300X accelerator. Intel's Foveros 3D integration technology, using micro-bumps with 36 μm pitch, stacks a 10 nm compute tile atop a 22 nm I/O die with a vertical interconnect density of **10,000 connections per mm²**, providing the equivalent system functionality of a monolithic die at a fraction of the manufacturing cost and with improved per-chiplet yield (Intel Corporation, 2022).

Figure 6.1 presents a cross-sectional comparison of planar MOSFET, FinFET, GAA nanosheet FET, and molecular junction device architectures, illustrating the evolution of transistor electrostatic control

SRR Publicizing Research

mechanisms and the dimensional scales characteristic of each technology generation.

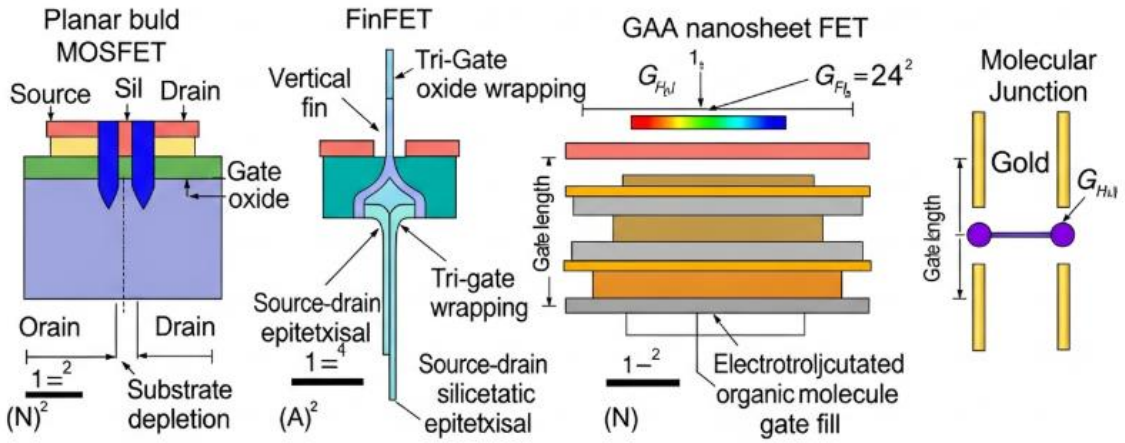

Figure 6.1: *Cross-sectional comparison of planar MOSFET, FinFET, GAA nanosheet FET, and molecular junction architectures, illustrating the evolution of electrostatic gate control and representative channel dimensions across transistor technology generations.*

6.3 Advanced DSP Systems and Applications

6.3.1 High-Performance DSP in AI Systems and Communication Technologies

The acceleration of AI workloads has driven the development of DSP architectures that integrate classical signal conditioning and feature extraction operations directly with neural network inference engines in a unified, tightly coupled processing pipeline. Modern AI inference SoCs, exemplified by Apple's A17 Pro Neural Engine, Google's Edge TPU, and Qualcomm's Cloud AI 100, implement heterogeneous processing hierarchies where dedicated DSP front-ends perform data acquisition, filtering, and spectral analysis while neural network accelerators execute the subsequent inference computation, with both subsystems sharing on-chip memory through a high-bandwidth interconnect fabric. The Apple A17 Pro Neural Engine achieves **35**

ISBN 978-816860178-9

TOPS of inference throughput at under 5 W total system power, enabled by a combination of 3 nm FinFET transistor density, 4-bit weight quantization, and sparsity-aware computation that skips zero-valued multiplications (Apple Inc., 2023).

The integration of advanced DSP capabilities with 5G and emerging 6G communication technology demands signal processing throughputs and latencies that push the boundaries of current hardware implementations. A 5G NR millimeter-wave (mmWave) base station operating at 100 GHz with 2 GHz channel bandwidth and 256-antenna massive MIMO requires real-time processing of **524,288 complex samples per second** across all antenna channels simultaneously, with beamforming weight computation latency below 125 µs to track mobile user equipment at vehicular speeds. These requirements are met in commercial 5G baseband chips such as Qualcomm's X65 modem through a combination of dedicated FFT accelerator arrays, matrix inversion engines for MIMO detection, and LDPC decoder clusters, collectively integrating over 5 billion transistors dedicated to baseband DSP functions. The energy efficiency of these implementations—measured in picojoules per bit of processed data—has improved by approximately **10× between the first 5G deployments in 2019 and the 2023 generation**, driven by both process node scaling and architectural optimization (Qualcomm Technologies, 2023).

Real-time embedded DSP applications in automotive, industrial, and medical domains impose additional constraints beyond raw throughput, requiring deterministic latency bounds, functional safety certification, and operation across extreme environmental conditions. Automotive radar DSP for Level 4 autonomous driving processes data from multiple 77 GHz FMCW radar sensors simultaneously,

performing range-Doppler processing, CFAR detection, and multi-target tracking with a maximum end-to-end latency of **50 ms** from sensor acquisition to track output—a budget that must accommodate FFT processing of chirp sequences containing 512 samples across 256 virtual antenna channels. NXP's S32R automotive radar processor achieves this with a dedicated radar DSP subsystem comprising four lockstep processor cores with hardware error correction, an integrated FFT accelerator capable of 2048-point transforms in 3.2 µs, and ISO 26262 ASIL-D functional safety certification ensuring correct operation in the presence of single-event upsets from cosmic ray particles (NXP Semiconductors, 2022).

Table 6.1: Performance Metrics of Advanced DSP Systems Across Application Domains

Application Domain	Processing Throughput	Latency Requirement	Power Envelope
5G NR mmWave Baseband	524K complex samples/sec	< 125 µs	8–15 W
Automotive Radar DSP	256-ch × 512-pt FFT/frame	< 50 ms	5–10 W
AI Neural Engine (Mobile)	35 TOPS inference	< 10 ms	2–5 W
Medical Ultrasound DSP	128-ch beamforming	< 1 ms	3–8 W

6.3.2 Multimedia Processing, Edge Computing, and Embedded DSP Integration

The proliferation of high-resolution multimedia content—4K and 8K video streaming, spatial audio, augmented reality overlays, and real-time video conferencing with AI-driven enhancement—has created a

ISBN 978-816860178-9

class of embedded DSP applications requiring unprecedented combinations of computational density, memory bandwidth, and energy efficiency within the thermal and power constraints of consumer devices. Modern video codec implementations supporting H.265 (HEVC) and AV1 compression standards employ DSP algorithms of substantial complexity: AV1 encoding of an 8K60 video stream requires approximately **100 billion operations per second**, including transform coding (DCT/ADST up to 64×64 blocks), motion estimation across reference frames, in-loop filtering, and entropy coding, implemented in dedicated video codec hardware blocks that achieve encoding throughputs of 240 fps for 4K content within a power budget of 2–4 W on ARM Mali-V78 and Apple ProRes video encoder silicon (Bankoski et al., 2011).

Edge computing architectures distribute DSP and AI inference workloads from centralized cloud servers to devices physically proximate to the data source, reducing communication latency, alleviating network bandwidth pressure, and addressing privacy concerns associated with transmitting raw sensor data to remote servers. The DSP requirements of edge inference are characterized by heterogeneous workloads—including keyword spotting, image classification, anomaly detection, and predictive maintenance—that must be executed on embedded processors with power budgets ranging from **1 mW for always-on voice detection** to 10 W for intelligent camera systems. ARM's Ethos-U85 neural processing unit, designed for microcontroller-class edge inference, achieves 4 TOPS within a 500 mW power envelope using a 512-wide MAC array with structured sparsity exploitation, enabling real-time execution of mobilenet-class image classification networks with 20 ms latency on battery-powered IoT devices (ARM Ltd., 2023).

Figure 6.2 illustrates the heterogeneous edge computing DSP system architecture, depicting the signal acquisition front-end, multi-domain DSP processing pipeline, on-chip AI inference accelerator, and communication interface layers characteristic of a next-generation intelligent edge sensor node.

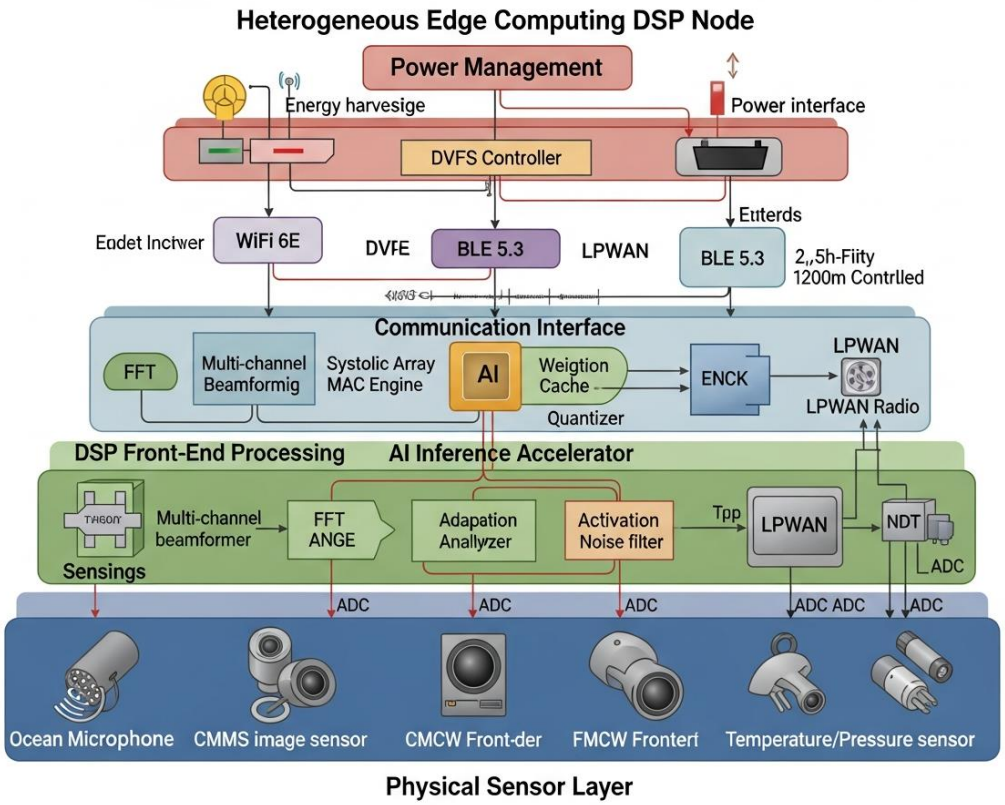

Figure 6.2: Heterogeneous edge computing DSP node architecture illustrating the signal acquisition front-end, multi-domain DSP processing pipeline, AI inference accelerator, communication interfaces, and energy-aware power management subsystem.

6.4 Future Trends and Research Directions

6.4.1 Neuromorphic Computing, 6G Integration, and Heterogeneous Systems

Neuromorphic computing is an emerging computational paradigm that draws architectural inspiration from the structure and operation of biological neural systems, implementing computation through

ISBN 978-816860178-9

networks of spiking neurons and plastic synapses that communicate via sparse, asynchronous voltage pulses rather than synchronized clock-driven binary logic operations. The fundamental advantage of neuromorphic architectures for signal processing applications lies in their intrinsic temporal coding capability and event-driven operation: a neuromorphic auditory processing system consuming 50 µW can continuously monitor acoustic environments for target sound patterns, activating energy-intensive processing only when relevant events occur, compared to a conventional DSP system that must maintain constant clock activity at milliwatt-level power. Intel's Loihi 2 neuromorphic research chip, fabricated in Intel's 4 nm Intel 4 process, integrates **1 million programmable neurons** and 120 million synapses on a single die with a total active power below 1 W, demonstrating sparse convolutional inference at 10–50× better energy efficiency than equivalent GPU implementations for event-driven sensor processing workloads (Davies et al., 2021).

The standardization process for 6G wireless communication, targeting commercial deployment around 2030, is driving DSP research into frequency bands, waveform designs, and multiple access schemes that demand processing capabilities far beyond current 5G implementations. 6G is anticipated to operate across a spectrum spanning sub-6 GHz, millimeter-wave (30–300 GHz), and sub-terahertz (100–300 GHz) bands simultaneously, with per-link data rates exceeding **1 Tbps** and air interface latencies below 100 µs—ten times higher throughput and ten times lower latency than 5G NR peak specifications. The DSP implications are immense: sub-terahertz OFDM signals with 20 GHz channel bandwidth require ADC sampling rates of 50–100 GS/s and FFT processors operating on 65,536-point transforms with update rates measured in

microseconds. Holographic radio, a 6G candidate technology that exploits reconfigurable intelligent surfaces (RIS) with thousands of antenna elements to shape the propagation environment, requires real-time channel estimation and beamforming weight computation across matrices of unprecedented dimension, demanding AI-assisted DSP algorithms that can extract channel structure from compressed measurements far below the Nyquist sampling rate (Tariq et al., 2020).

Heterogeneous system design, integrating diverse compute elements—CPU, GPU, DSP, NPU, FPGA fabric, and analog mixed-signal blocks—within a unified chiplet-based package, is rapidly becoming the dominant architectural paradigm for high-performance electronic systems. The package-level integration enabled by TSMC's System on Integrated Chips (SoIC) technology and Intel's EMIB (Embedded Multi-die Interconnect Bridge) allows chiplets from different process nodes and even different foundries to be combined with die-to-die interconnect bandwidths exceeding **2 Tbps/mm²** at energy efficiencies of 0.5 pJ/bit—approaching the performance of on-chip global wiring. AMD's Instinct MI300X, integrating 13 chiplets comprising 3 nm compute dies and 5 nm HBM memory controller dies in a unified package with 192 GB of HBM3 memory, demonstrates the system-level performance achievable through heterogeneous integration: **1.3 TB/s memory bandwidth** and 383 TOPS of INT8 inference throughput within a 750 W thermal design power (AMD, 2023).

ISBN 978-816860178-9

6.4.2 Sustainable Electronics, Energy Efficiency, and Research Outlook

Table 6.2: Energy Efficiency Projections for Emerging Computing Technologies (2025–2035)

Technology	Energy per Operation	Projected Density	Technology Readiness
2 nm GAA CMOS Logic	0.5 aJ / logic op	500 MTr/mm²	Production 2025
Neuromorphic (Loihi-class)	10 fJ / synaptic op	1M neurons/chip	Research / Early adoption
Optical Interconnect (on-chip)	0.1 pJ / bit	10 Tbps/mm²	Research prototype
Superconducting Logic (RSFQ)	0.001 aJ / logic op	Limited by cooling	Laboratory stage

The sustainability imperative in semiconductor technology has emerged as a critical research and engineering priority, driven by the escalating energy consumption of global data center and communication infrastructure. Data centers currently consume approximately **200–250 TWh of electricity annually** worldwide—roughly 1% of global electricity consumption—and AI training workloads are projected to increase this figure substantially through the decade. The carbon footprint of semiconductor manufacturing itself is also substantial: fabricating a single 300 mm wafer in a leading-edge process requires approximately 2,000 liters of ultra-pure water and consumes 2–4 MWh of electricity, with perfluorocarbon (PFC) etch gases contributing to greenhouse gas emissions equivalent to thousands of tons of CO_2 per year at a large wafer fab (Andrae & Edler, 2015).

Energy-proportional computing—where system power consumption scales linearly with computational workload rather than maintaining near-peak consumption even at low utilization—is a fundamental design objective for sustainable electronic systems. Dynamic voltage and frequency scaling (DVFS) implemented in conjunction with workload prediction using on-chip ML models achieves energy-proportionality factors of **0.85–0.95** in modern mobile SoCs, compared to 0.3–0.4 in conventional server processors. Near-threshold computing (NTC) designs, operating at supply voltages within 100 mV above the transistor threshold voltage (approximately 0.4–0.5 V in 7 nm FinFET), reduce dynamic power by **4–9×** compared to nominal voltage operation at the cost of 5–10× reduction in operating frequency, making NTC suitable for error-tolerant DSP workloads in IoT and wearable applications where energy is the primary constraint (Dreslinski et al., 2010).

The convergence of photonic computing with electronic DSP systems represents a particularly promising research direction for breaking the energy and bandwidth walls of conventional electronic interconnects and arithmetic. Silicon photonic integrated circuits, fabricated in standard CMOS-compatible processes with germanium photodetector integration, achieve optical modulation bandwidths of 50–100 GHz per channel with modulation energies below **1 fJ/bit**—more than 100× more energy-efficient than equivalent electrical signaling at comparable data rates. Optical neural network inference using Mach-Zehnder interferometer meshes has been experimentally demonstrated at speeds of terahertz multiply-accumulate operations per second with femtojoule-per-MAC energy consumption, though the precision of optical computation is currently limited to 4–6 effective

ISBN 978-816860178-9

bits by device imperfections and noise, restricting applications to workloads tolerant of quantization effects (Shen et al., 2017).

6.5 Summary

This section has examined the frontier of nanoelectronics and DSP systems across the device, circuit, architecture, and application layers, establishing a cohesive picture of the technological trajectory shaping the next decade of semiconductor innovation. The evolution from FinFET through GAA nanosheet transistors to beyond-CMOS device concepts including CNFETs, NC-FETs, and molecular junctions was analyzed in terms of electrostatic performance, energy efficiency, and manufacturing readiness. Advanced DSP system implementations in AI inference, 5G mmWave baseband, automotive radar, and edge computing were quantified with representative performance metrics, illustrating the breadth and depth of real-time signal processing demands. The forward-looking research directions of neuromorphic computing, 6G DSP integration, heterogeneous chiplet architectures, and sustainable electronics were synthesized into a coherent outlook that underscores the continued vitality and societal importance of innovation at the intersection of nanoelectronics and digital signal processing.

References

[1] AMD. (2023). *AMD Instinct MI300X accelerator technical specifications*. Advanced Micro Devices. https://www.amd.com/en/products/accelerators/instinct/mi300/mi300x.html

[2] Andrae, A. S., & Edler, T. (2015). On global electricity usage of communication technology: Trends to 2030. *Challenges, 6*(1), 117–157. https://doi.org/10.3390/challe6010117

[3] Apple Inc. (2023). *A17 Pro chip overview: Neural engine and machine learning*. Apple Developer Documentation. https://developer.apple.com/documentation/apple-silicon

[4] ARM Ltd. (2023). *Arm Ethos-U85 neural processing unit product brief*. ARM Technical Documentation. https://developer.arm.com/Processors/Ethos-U85

[5] Arute, F., Arya, K., Babbush, R., & Martinis, J. M. (2019). Quantum supremacy using a programmable superconducting processor. *Nature, 574*(7779), 505–510. https://doi.org/10.1038/s41586-019-1666-5

[6] Bankoski, J., Koleszar, J., Quillio, L., & Salonen, J. (2011). VP8 data format and decoding guide. *IETF RFC 6386*, Internet Engineering Task Force.

[7] Davies, M., Wild, A., Orchard, G., & Taba, B. (2021). Advancing neuromorphic computing with Loihi: A survey of results and outlook. *Proceedings of the IEEE, 109*(5), 911–934. https://doi.org/10.1109/JPROC.2021.3067593

[8] Desai, S. B., Madhvapathy, S. R., Sachid, A. B., & Javey, A. (2016). MoS_2 transistors with 1-nanometer gate lengths. *Science, 354*(6308), 99–102. https://doi.org/10.1126/science.aah4698

[9] Dreslinski, R. G., Wieckowski, M., Blaauw, D., & Mudge, T. (2010). Near-threshold computing: Reclaiming Moore's law through energy efficient integrated circuits. *Proceedings of the IEEE, 98*(2), 253–266. https://doi.org/10.1109/JPROC.2009.2034764

[10] Ferain, I., Colinge, C. A., & Colinge, J. P. (2011). Multigate transistors as the future of classical metal-oxide-semiconductor field-effect transistors. *Nature, 479*(7373), 310–316. https://doi.org/10.1038/nature10676

[11] Intel Corporation. (2022). *Intel Foveros 3D advanced packaging technology overview*. Intel Foundry Services Technical Brief. https://www.intel.com/content/www/us/en/foundry/packaging.html

[12] Ionescu, A. M., & Riel, H. (2011). Tunnel field-effect transistors as energy-efficient electronic switches. *Nature, 479*(7373), 329–337. https://doi.org/10.1038/nature10679

ISBN 978-816860178-9

[13] Lundstrom, M., & Jeong, C. (2013). *Nanoscale transistors: Device physics, modeling and simulation*. Springer.

[14] NXP Semiconductors. (2022). *S32R automotive radar processor product brief*. NXP Technical Documentation. https://www.nxp.com/products/processors-and-microcontrollers/s32-automotive-platform/s32r

[15] Qualcomm Technologies. (2023). *Snapdragon X65 5G modem-RF system technical overview*. Qualcomm Product Brief. https://www.qualcomm.com/products/technology/modems/snapdragon-x65-5g-modem-rf-system

[16] Ratner, M. (2013). A brief history of molecular electronics. *Nature Nanotechnology, 8*(6), 378–381. https://doi.org/10.1038/nnano.2013.110

[17] Shen, Y., Harris, N. C., Skirlo, S., & Soljačić, M. (2017). Deep learning with coherent nanophotonic circuits. *Nature Photonics, 11*(7), 441–446. https://doi.org/10.1038/nphoton.2017.93

[18] Tariq, F., Khandaker, M. R., Wong, K. K., & Imran, M. A. (2020). A speculative study on 6G. *IEEE Wireless Communications, 27*(4), 118–125. https://doi.org/10.1109/MWC.001.1900488

[19] TSMC. (2023). *TSMC N2 nanosheet technology overview and roadmap*. Taiwan Semiconductor Manufacturing Company. https://www.tsmc.com/english/dedicatedFoundry/technology/logic/l_2nm

ISBN 978-816860178-9

Innovations in VLSI Architecture and Digital Signal Processing
April 2026

Dr. M. KAMARAJAN received his B.E degree in Electronics and Communication Engineering from Anna University, MIT Campus, Chennai and his M.E Degree in Applied Electronics from Jerusalem College of Engineering, Anna University, Chennai. He obtained his Ph.D. in Electronics and Communication Engineering from Anna University, Chennai. He is currently working as an Assistant Professor in the Department of Electronics and Communication Engineering at Vels Institute of Science, Technology & Advanced Studies (VISTAS), Chennai. His research interests include Machine Learning, Image Processing, Biomass waste optimization, Embedded Systems and IoT. He has published more than 20 research papers/articles in Scopus indexed and Web of Science Journals. He has over 25 years of teaching experience and has supervised more than 25 UG and PG scholars.

Mrs. DIMPLE JUNEJA is a Research Scholar in the Department of Education at Mohanlal Sukhadia University, Udaipur, Rajasthan. She holds multiple qualifications, including M.Phil. in Commerce, M.Com., M.Ed., MBA (Finance & HR), M.A. in Economics, and a Certificate in Guidance. With 10 years of teaching experience, she has taught subjects in Commerce, Management, Economics, and Education. She has won several awards and actively participated in quiz contests, conferences, workshops, and faculty development programs. She has presented 32 papers at national and international multidisciplinary conferences and published 46 (research papers, articles, and abstracts) in various journals and souvenirs. She has also served as the editor of 50 books and 5 souvenirs. Dimple is a lifetime member of several professional organizations.

Dr. A. YOGESHWARAN received his B.E. in Electronics and Communication Engineering from M.A.M. College of Engineering, Anna University, Chennai, in 2007, and his M.E. in Communication Systems from Dhanalakshmi Srinivasan Engineering College, Anna University, Trichy, in 2011. He earned his Ph.D. in Information and Communication Engineering from Anna University, Chennai, in 2023. With 15 years of teaching experience, he currently serves as an Assistant Professor in the Department of Electronics and Communication Engineering at Dhanalakshmi Srinivasan Engineering College (Autonomous), Perambalur. His research interests include microstrip patch antennas, wireless communication, and digital image processing. He has guided 13 postgraduate students and 26 undergraduate batches, published 23 journal papers, presented at 11 conferences, and authored five academic books.

Dr. S. MUTHURAJAN teaches Electrical and Electronics Engineering subjects in Academy of Maritime Education and Training (AMET), Deemed to be University, Kanathur, Chennai. He has completed his B.E in National Engineering College, Kovilpatti. He did his Post Graduate in Industrial Electronics from the Maharaja Sayajirao University of Baroda, Gujarat and he was awarded a Ph.D from St. Peter's Institute of Higher Education and Research, Chennai. He has published various technical papers in reputed journals. His experience in teaching career helps the students enhance their Engineering knowledge.

SCIENTIFIC RESEARCH REPORTS

(A Book Publisher, approved by Govt. of India)

I Floor, S S Nagar, Chennai - 600 087,
Tamil Nadu, India.
editors@srrbooks.in, contact@srrbooks.in
www.srrbooks.in

ISBN 978-816860178-9